Chemistry–A European Journal
Review
doi.org/10.1002/chem.202303987
Chemistry Europe
European Chemical Societies Publishing

www.chemeurj.org

Magnetic–Plasmonic Nanocomposites as Versatile Substrates for Surface–enhanced Raman Scattering (SERS) Spectroscopy

Ecem Tiryaki,*[a] Tolga Zorlu,*[b] and Ramon A. Alvarez-Puebla*[c, d]

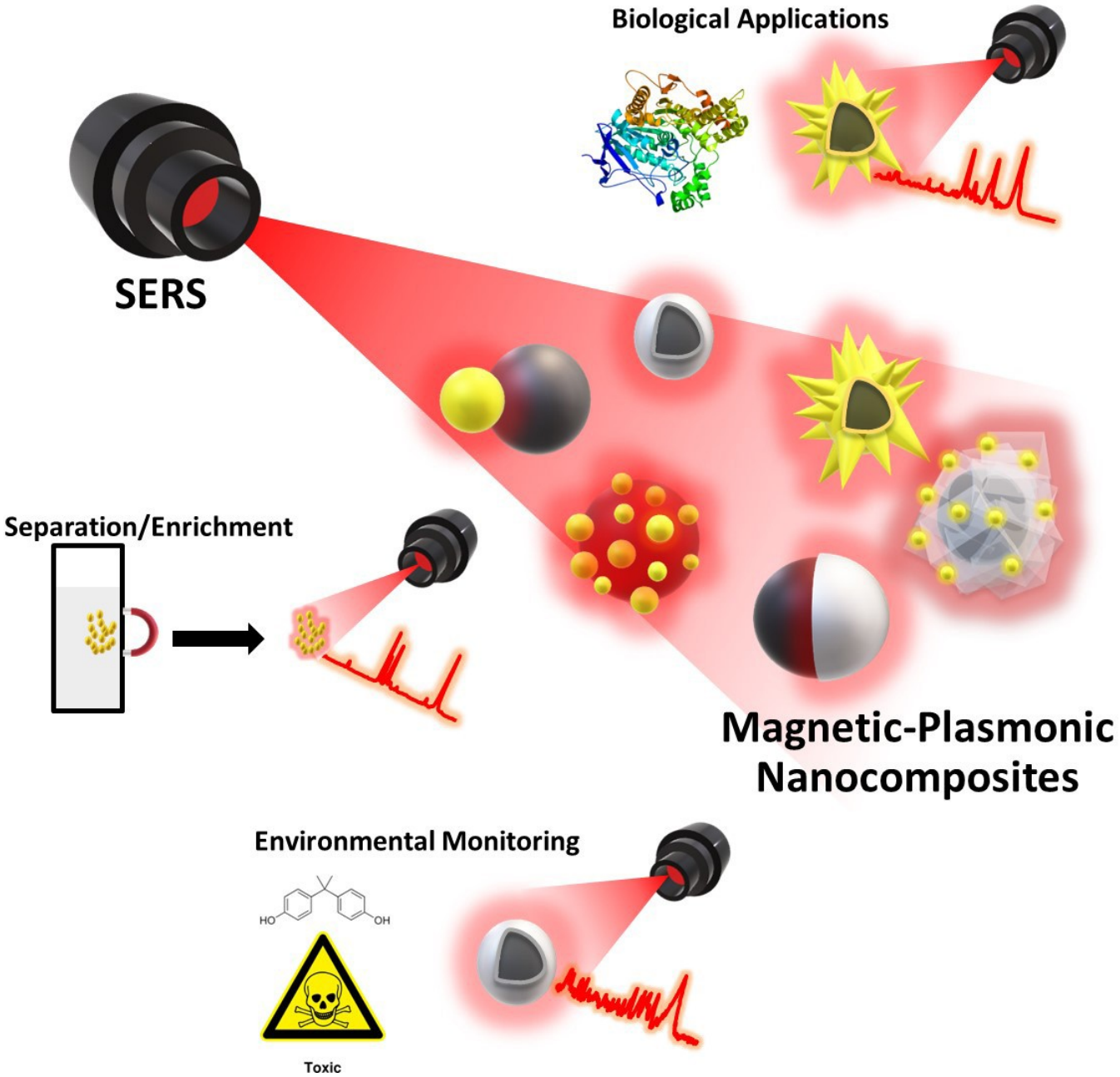

Surface–enhanced Raman scattering (SERS) spectroscopy, a highly sensitive technique for detecting trace–level analytes, relies on plasmonic substrates. The choice of substrate, its morphology, and the excitation wavelength are crucial in SERS applications. To address advanced SERS requirements, the design and use of efficient nanocomposite substrates have become increasingly important. Notably, magnetic–plasmonic (MP) nanocomposites, which combine magnetic and plasmonic properties within a single particle system, stand out as promising nanoarchitectures with versatile applications in nanomedicine and SERS spectroscopy. In this review, we present an overview of MP nanocomposite fabrication methods, explore surface functionalization strategies, and evaluate their use in SERS. Our focus is on how different nanocomposite designs, magnetic and plasmonic properties, and surface modifications can significantly influence their SERS-related characteristics, thereby affecting their performance in specific applications such as separation, environmental monitoring, and biological applications. Reviewing recent studies highlights the multifaceted nature of these materials, which have great potential to transform SERS applications across a range of fields, from medical diagnostics to environmental monitoring. Finally, we discuss the prospects of MP nanocomposites, anticipating favorable developments that will make substantial contributions to various scientific and technological areas.

1. Introduction

Surface–enhanced Raman scattering (SERS) spectroscopy is a sensitive analytical technique widely used for detecting analytes at ultra–trace levels.[1] It relies on the significant enhancement of Raman signals from analytes that are adsorbed onto or in close proximity to a plasmonic surface. This enhancement is attributed to the intense electromagnetic field generated by localized surface plasmons (LSPs), resulting from the interaction between plasmonic nanoparticles (NPs) such as gold, silver, and copper, and incident light.[2] Consequently, even minute quantities of analytes can be easily and rapidly identified and quantified without the need for additional sample preparation techniques.

While simple bare plasmonic metals of various types and morphologies may suffice for certain SERS-based applications, versatile and reproducible substrates with exceptional performance are crucial for practical applications. In this context, integrating multiple elements or materials to create nanoalloy or nanocomposite substrates emerges as a remarkable strategy. By combining different materials, significant enhancements in the SERS performance of plasmonic substrates can be achieved.[3] Similarly, employing plasmonic–plasmonic nanoalloys, such as Au/Ag structures with enhanced local EM fields, sensitivity, and chemical stability, has proven to be highly advantageous for signal amplification when compared to their monometallic counterparts.[4] There is a growing prevalence of hybrid nanocomposites, particularly those combining plasmonic metals with different transition metals, which significantly expand the capabilities of SERS.[4a] Among these transition metals, those with magnetic properties are especially popular for integration with plasmonic NPs.[5] This combination allows for the creation of nanocomposites that can be externally excited and possess the ability to control and manipulate light. Magnetic–plasmonic (MP) nanocomposites have found extensive application in nanomedicine as theragnostic materials,[6] primarily due to their biocompatibility, potential for direct targeting, and suitability for techniques like photothermal therapy. Moreover, their use in various SERS-based applications broadens their potential.

For instance, in separation processes, these nanocomposites demonstrate a unique ability to efficiently extract and isolate analytes from complex environments, thereby streamlining sample preparation in various analytical contexts.[7] In environmental monitoring, their exceptional sensitivity enables the detection of trace–level pollutants, heavy metals, and contaminants in air, water, and soil. This contributes significantly to our understanding of environmental health and pollution mitigation efforts.[8] Additionally, the ease of retrieving these particles from the environment using a magnet for repeated use highlights their eco–friendly and cost–effective nature compared to SERS substrates that only exhibit plasmonic properties.[23]

In biological applications, MP nanocomposites are invaluable due to their magnetic properties, which allow for precise manipulation and targeting in biological systems. They are crucial tools for drug delivery, cell sorting, and biomolecule detection, with a particular promise in biomedical research for the sensitive and specific detection of biomarkers, pathogens, and cellular components. The challenges of signal repeatability and sensitivity, often faced in systems relying solely on plasmonic NPs, can be effectively addressed by incorporating magnetic separation and enrichment functions.[24] Furthermore, their ability to enhance Raman signals of biological molecules offers unprecedented insights into cellular processes and disease diagnostics.[9]

[a] Dr. E. Tiryaki
Nanomaterials for Biomedical Applications. Italian Institute of Technology (IIT), Geneva, 16163 Geneve, Italy.
E-mail: ecem.tiryaki@iit.it
[b] Dr. T. Zorlu
Faculty of Chemistry, Institute of Functional Materials and Catalysis, University of Vienna, Währingerstr. 42, A-1090 Vienna, Austria
E-mail: tolga.zorlu@univie.ac.at
[c] Prof. Dr. R. A. Alvarez-Puebla
Department of Inorganic and Physical Chemistry, Universitat Rovira i Virgili, C/Marcel·lí Domingo s/n, 43007 Tarragona, Spain
E-mail: ramon.alvarez@urv.cat
[d] Prof. Dr. R. A. Alvarez-Puebla
ICREA, Passeig Lluis Companys 23, 08010 Barcelona, Spain

Finally, the capacity of a nanocomposite assembly, guided by a magnetic field, to prevent uncontrollable particle aggregation common in noble metal NPs and to enhance the density of hot spots between plasmonic entities, significantly boosts signal amplification. With these advantages, magnetic–plasmonic nanocomposites enable the detection of target molecules at ultra–low concentrations, setting them up to revolutionize SERS technology across various fields, from environmental conservation to medical research, as they become more tailored to specific applications.

In this review, we offer a detailed summary of the most common synthesis methods for magnetic–plasmonic (MP) nanocomposites, their varied approaches to surface functionalization, and their effectiveness as substrates in Surface–enhanced Raman scattering (SERS) applications. We have thoroughly investigated the synthesis of MP nanocomposites, paying special attention to how their morphology, composition, and surface characteristics influence their magnetic and optical properties. This analysis clarifies why certain nanocomposite structures are preferred for different SERS-based applications, providing readers with valuable insights into the suitability of various structures for specific SERS methodologies. Additionally, we delve into specific applications of SERS where these nanoarchitectures demonstrate their effectiveness, highlighting their advanced capabilities and frequent use in state-of-the-art analytical scenarios. The review aims to present a comprehensive understanding of MP nanocomposites, emphasizing how their unique properties can be harnessed for enhanced performance in SERS applications, thereby contributing to the advancement of this field.

2. Magnetic–Plasmonic Nanocomposites

Magnetic–plasmonic (MP) nanocomposites are multifunctional structures created by integrating materials with both magnetic and plasmonic properties. Their synthesis can be achieved through either a single–step or multi–step process. In a single–step process, both components are added and grown simultaneously within the reaction medium. In multi–step processes, each component is synthesized separately. Typically, the first step involves synthesizing magnetic nanoparticles (NPs), usually derived from transition metals like iron, nickel, or cobalt.[10] Plasmonic materials often consist of metals like gold or silver, known for their plasmonic properties. These materials can be shaped into various morphologies, such as single–crystal nanospheres,[11] nanorods (NRs),[12] nanowires (NWs),[13] nanodisks,[14] using different synthesis methods. In the second step, magnetic NPs serve as the starting point, onto which plasmonic materials are added to form MP nanocomposites. This can be achieved in two primary ways. The first involves synthesizing magnetic and plasmonic NPs separately and then combining them through chemical bonding or electrostatic interactions.[15] This chemical bonding of plasmonic NPs onto magnetic materials can be facilitated using surface functionalization techniques or chemical binding agents. Alternatively, physical mixing of the NPs within a polymer or inorganic matrix can also be employed.[16] The second approach involves functionalizing the surface of magnetic NPs and then growing a plasmonic shell using various plasmonic precursors and reducing agents.[17] Depending on the specific SERS application, these nanocomposites can also be transformed into anisotropic morphologies using post–modification methods.[18]

An essential aspect of MP nanocomposite production is the interaction between the magnetic and plasmonic components.

Ecem Tiryaki obtained her MSc. Degree in 2017, from the Yildiz Technical University, Turkey. In 2022, she received her PhD from the University of Vigo, where she focused on the design of hybrid plasmonic and magnetic nanostructures. She collaborated with the Parak's Group in Hamburg, Germany, in magnetic particle–cell interactions. Since May 2023, she has worked as a Postdoctoral Researcher at the Italian Institute of Technology (IIT) in Genova, Italy. Her current research subject is the synthesis of magnetic–plasmonic nanostructures for magnetic manipulation and biological.

Tolga Zorlu earned his PhD degree in 2023, from the Universitat Rovira i Virgili, under the supervision of Prof. Ramon A. Alvarez-Puebla and Prof. Miguel A. Correa-Duarte. His research is focused on the development of advanced colloidal plasmonic nanosensors for SERS. Throughout his doctoral work, he extensively explored the utilization of metal–organic and covalent–organic frameworks, integrating them into plasmonic nanostructures to enhance sensitivity in both detection and catalysis studies. Since December 2023, he has worked as a Postdoctoral Researcher at Universität Wien in Vienna, Austria.

Ramon A. Alvarez-Puebla is an ICREA Professor at the Universitat Rovira i Virgili in Tarragona. He holds a BSc in Chemistry (Universidad de Navarra, 2000) and a PhD in Surface Science (Universidad Publica de Navarara, 2003). He was postdoc at University of Windsor (Windsor, ON, Canada) and General Motors Corporation (Warren, MI, USA) and worked as Research Officer at the National Institute for Nanotechnology of the National Research Council of Canada (Edmonton, AB, Canada) and as Associate Professor at the Universidade de Vigo.

This interaction can affect the distribution of plasmonic material on the magnetic core and alter the plasmonic resonance properties. Additionally, it is crucial that the magnetic NPs retain their magnetic characteristics after the addition of the plasmonic component to ensure easy external manipulation. Therefore, a careful examination of this interaction is key to achieving optimal magnetic and plasmonic properties in the nanocomposites for effective use in SERS-based applications.

2.1. General Synthesis Strategy for Magnetic Nanoparticles

Various approaches exist in the synthesis of magnetic NPs, with basic methods typically including chemical approaches such as co-precipitation,[19] thermal decomposition,[20] sol–gel,[21] hydrothermal and solvothermal methods,[22] as well as green synthesis approaches (Figure 1).

Since its initial report by Massart in 1982, the co-precipitation method has been extensively used for synthesizing Fe_3O_4 magnetic NPs.[23] This method involves the simultaneous precipitation of two or more metal salts in an alkaline solution.[24] The process begins with the rapid mixing of metal ion solutions under controlled conditions, leading to the formation of a mixed metal hydroxide precipitate. This precipitate is then subjected to additional processes such as washing, drying, and calcination to obtain the desired magnetic NPs. The co-precipitation method offers several advantages in the synthesis of magnetic NPs. Firstly, it allows for controlled composition by adjusting the ratio of metal salts.[25] Secondly, it enables the synthesis of NPs with specific sizes and shapes, which are essential for achieving the desired magnetic properties. Furthermore, this method can be easily scaled up for large-scale production. The success of the co-precipitation method depends on multiple factors. The choice of metal salts, their concentrations, and the pH of the reaction solution significantly influence the properties of the resulting magnetic NPs. The reaction temperature and duration also affect the particle size, crystalline structure, and magnetic behavior. Precise control over these parameters allows for customization of the size distribution, composition, and magnetic properties of the magnetic NPs. In addition to these primary factors, seemingly minor variables can also significantly impact the characteristics of the magnetic NPs synthesized using the co-precipitation method. For example, Gahrouei et al. (2020) employed ultrasonic irradiation–assisted co-precipitation to synthesize γ-Fe_2O_3 and Fe_3O_4 NPs.[26] Their findings indicate that ultrasonic irradiation produces smaller, well–dispersed magnetic NPs. Generally, researchers opt for this method due to its simplicity

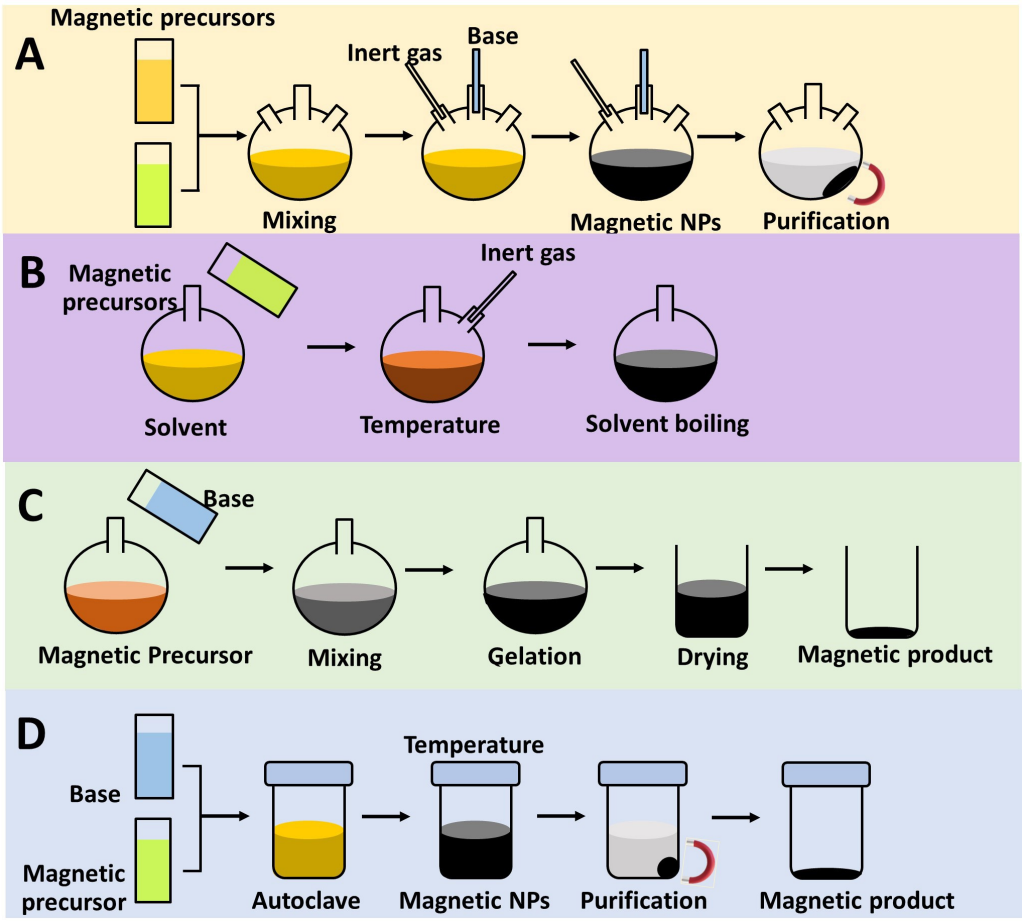

Figure 1. Schematic illustration of common synthesis strategies of magnetic NPs: A) Co-precipitation, B) Thermal decomposition, C) Sol–gel, and D) Hydrothermal method.

and cost–effectiveness, but it is important to note that there are limitations, including challenges in controlling particle properties, issues with agglomeration, and potential impurities.

The thermal decomposition method is a significant technique for synthesizing magnetic NPs, noted for its precise control over particle size, shape, and composition.[27] This process involves heating metal precursors, typically organometallic compounds, to high temperatures under conditions of inert gas or solvent. As the temperature increases, these precursors decompose, initiating nucleation and subsequent growth of NPs. The method's-controlled nature facilitates the production of monodisperse magnetic NPs, tailored for specific magnetic properties, and suitable for various applications, including biomedicine and data storage. One of the key advantages of the thermal decomposition method is the production of NPs with a narrow size distribution, which enhances their performance across diverse technological and scientific fields. Additionally, adjustable reaction parameters allow for the creation of magnetically and thermally robust structures. This includes core/shell configurations with combined hard and soft components or diverse anisotropic morphologies, thus enhancing magnetic anisotropy and enabling their use in specialized applications. For example, Sartori et al. (2019) demonstrated this by synthesizing onion–like ferrite core/shell/shell magnetic NPs using a three-step thermal decomposition process.[28] They achieved a structure with an $Fe_{3-\delta}O_4$ core and an external shell, separated by a Co-ferrite interlayer. These NPs, with an average diameter of 16 nm, exhibited efficient magnetic anisotropy due to the hard–soft exchange coupling maintained by the thermal decomposition reaction conditions.

However, despite its precise control over NP properties, the thermal decomposition method has its challenges. It requires careful handling due to the high temperatures and complex process control involved. Additionally, the toxicity of organic solvents used, difficulty in scalability, and potential misalignment with green chemistry principles, particularly regarding eco–friendliness, are notable drawbacks of this method.

The sol–gel method is a chemical process used to synthesize magnetic NPs by converting metal oxides or other inorganic materials from a liquid solution to a gel state.[29] Known for its cost–effectiveness, simplicity, and controllability, this technique typically operates at low temperatures. The process involves two primary stages: initially, a solution is prepared, usually comprising a hydrolyzed metal precursor such as a metal alkoxide or metal salt. Then, this solution gradually undergoes condensation, leading to the formation of a gel. Chemical reactions within this gel result in a three–dimensional structure, facilitating control over the size and distribution of the NPs. Various parameters, including substitution cations,[30] annealing temperature,[31] pH value,[32] and other factors, play crucial roles in determining properties such as particle size, crystalline structure, surface characteristics, and magnetic properties. The sol–gel method is particularly effective in synthesizing magnetic NPs,[33] but the selection of metal precursors is key, as it influences the type and characteristics of the resultant magnetic material. A study by Rahimi et al. (2017)[34] illustrates this point well. They synthesized Nd–Fe–B oxide powders using chloride and nitrate precursors with varying pH values, observing that the pH significantly affected the phase, morphology, microstructure, and magnetic properties of the powders. Lower pH values led to smaller particle sizes and higher coercivity. Notably, powders made with chloride precursors had smaller sizes, higher saturation magnetization, and coercivity than those made with nitrate precursors. The next stage involves solidification through drying and sintering. Parameters associated with these steps, such as temperature, atmospheric conditions, and duration, significantly influence the NPs' size, crystalline structure, and magnetic behaviour. For example, a study by Zhou et al. (2022)[35] found that $Ni_{0.4}Zn_{0.2}Mn_{0.4}Fe_2O_4$ ferrites synthesized under nitrogen atmosphere or at higher temperatures exhibited larger sizes and better magnetic properties. In contrast, those synthesized at lower temperatures showed lower magnetic properties but better thermal stability. The drying process aims to remove the liquid component from the gel, resulting in a solid matrix. Sintering then promotes particle bonding and crystallization, leading to a well–defined crystal structure. By meticulously controlling the temperature, atmosphere, and duration during these stages, researchers can manipulate the final NP size, enhance crystallinity, and tailor the magnetic properties of the synthesized NPs.

The hydrothermal method, similar to the sol–gel approach, is highly effective for synthesizing magnetic NPs with customizable size, crystal structure, and magnetic properties.[36] Using specialized reaction vessels, reactions are conducted under high temperature and pressure, ensuring the production of desired outcomes while minimizing side reactions. The hydrothermal reaction conditions are crucial in determining both reaction efficiency and the quality of the resultant magnetic NPs. Precise control over parameters like precursor, temperature, and pressure allows for fine–tuning of size, morphology, crystallinity, and magnetic behavior.[37] For example, Torres–Gómez et al. (2019) observed that Fe_3O_4 NPs synthesized at 120, 140, and 160 °C through this method showed polyhedral or quasi–spherical, octahedral, and cubic morphologies, respectively.[38] Factors such as applied pressure, reaction time, and pH significantly influence the magnetic characteristics in this method.[39]

The solvothermal method, another robust technique, is used to synthesize magnetic NPs with precise control over their size, morphology, and crystalline structure.[40] In this process, a precursor solution containing metal salts or compounds is heated in an organic solvent medium within a high–pressure vessel. The high–pressure and temperature conditions favor nucleation and growth of NPs with distinct characteristics. The selection of solvent, temperature, and reaction duration enables the customization of the magnetic NPs' properties. Recently, Gavilán et al. (2023) developed an optimized solvothermal protocol to produce ferrite NPs with varied morphologies.[22b] By altering the type of aldehyde ligand, they achieved anisotropic shapes like nanocubes or nanostars, exhibiting narrow size distributions and high crystallinities, which are particularly beneficial for applications such as magnetic hyperthermia.

Lastly, green synthesis of magnetic NPs offers a promising and environmentally friendly alternative to conventional meth-

ods. This approach utilizes natural resources like plant extracts, microorganisms, and biocompatible compounds as reducing and stabilizing agents. Green synthesis reduces the use of hazardous chemicals and energy–intensive processes, aligning with sustainability and eco–friendliness principles. Moreover, magnetic NPs produced via green synthesis often exhibit excellent biocompatibility, making them suitable for biomedical applications such as drug delivery, hyperthermia therapy, and as MRI contrast agents.[41]

2.2. General Synthesis Strategy for Plasmonic Nanoparticles

Several methods are available for synthesizing plasmonic nanoparticles (NPs), each offering unique advantages depending on the desired NP properties, size, distribution, and optical characteristics. The most used methods include chemical reduction, hydrothermal/solvothermal methods, and green synthesis approaches (Figure 2), with the choice of method being contingent on the target NP features.

The chemical reduction method, particularly prominent in the synthesis of plasmonic NPs, is exemplified by the Turkevich method for Au NPs.[42] This well–known procedure involves heating aqueous gold salt, like HAuCl4, with a reducing agent such as citric acid.[43] Despite being over 70 years old, the Turkevich method remains a preferred technique for creating spherical, small–sized Au NPs (approximately 12–13 nm).[44] In contrast, the chemical synthesis of Ag NPs often involves ascorbic acid as a reducing agent and can require the incubation of $AgNO_3$ with a compound like NaCl.[45] This method facilitates the production of monodisperse plasmonic NPs and enables the synthesis of NPs with various sizes or morphologies through the seed–mediated approach, where reactions occur on the surfaces of existing plasmonic NPs.[46]

Hydrothermal and solvothermal methods also play a significant role in plasmonic NP synthesis.[47] These methods involve dissolving metal salts and reactants in a solvent, followed by processing in a hydrothermal reactor under high temperature and pressure. The hydrothermal method allows control over NP size, distribution, and crystal structure, while the solvothermal method emphasizes the solvent's role in influencing reaction conditions and NP properties. For example, Hao et al. (2022) demonstrated the impact of different solvents on the size and monodispersity of Au NPs using the oleylamine–reduced method.[48]

Green synthesis methods, using natural sources like plant extracts, biological materials, and biodegradable polymers, are gaining attention for their environmental sustainability.[49] These methods reduce the environmental impact and often result in NPs with enhanced biocompatibility. Plant extracts, for instance, act as reducing agents for metal ions, influencing the reaction rate and controlling NP properties. Biological processes from organisms like algae or fungi contribute to NP synthesis through the reduction and amalgamation of metal ions.[50] Biodegradable polymers in green synthesis offer control over NP synthesis and ensure biocompatibility.[51]

2.3. Fabrication of Magnetic–Plasmonic Nanocomposites

The fabrication of magnetic–plasmonic (MP) nanocomposites encompasses a range of methods and strategies (Figure 3). A

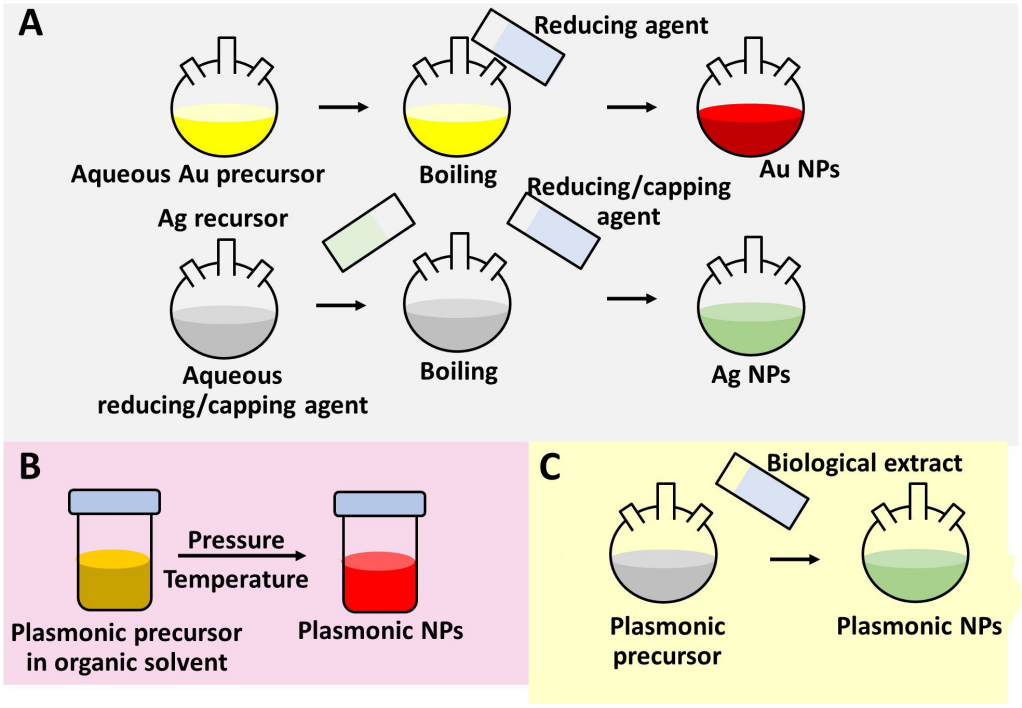

Figure 2. Schematic illustration of common synthesis strategies of plasmonic NPs: A) Reducing method, B) Solvothermal method, and C) Green synthesis method.

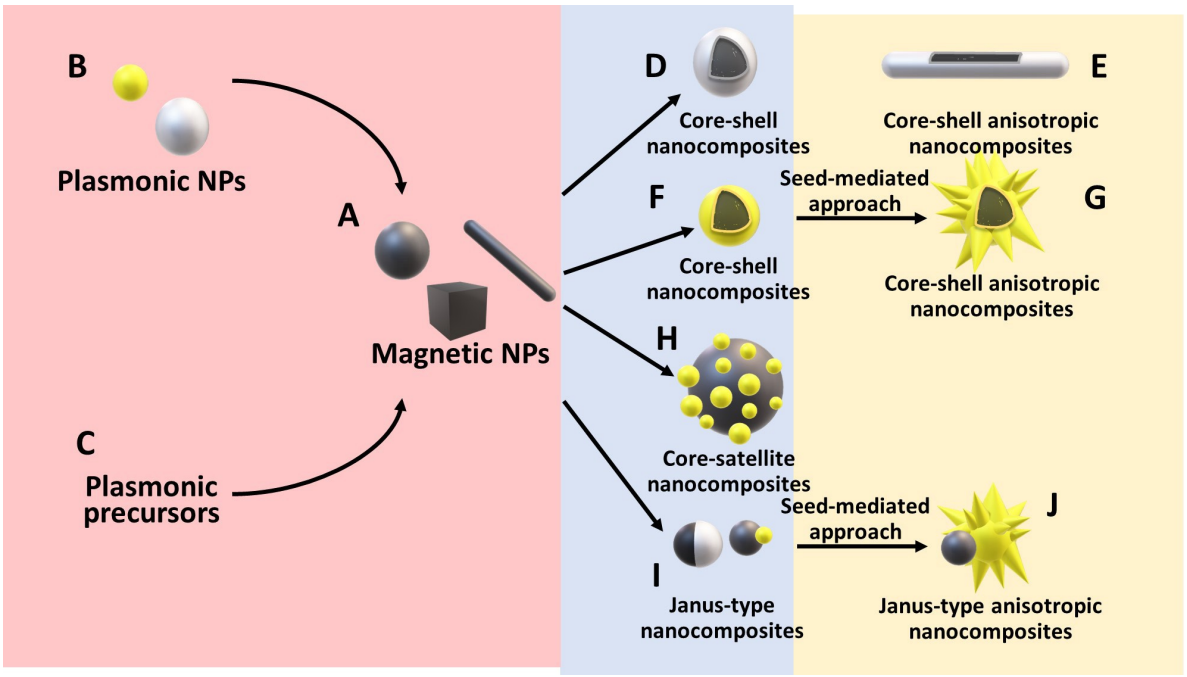

Figure 3. Schematic illustration of the fabrication of MP nanocomposites. In general, there are two primary strategies for obtaining MP nanocomposites: Magnetic NPs (A) that have different morphologies can be synthesized, and plasmonic NPs (B) can be deposited onto this structure through various methods. Additionally, in the second strategy, plasmonic precursors (C) can be grown onto magnetic NPs with the assistance of various reducing agents to form a shell. Both strategies can result in the formation of core–shell, core-satellite, or Janus–type MP nanocomposites (D, F, H, and I). Depending on the morphology of the initially used magnetic NPs, anisotropic core–shell nanocomposites can be obtained either in a single step (E) or novel anisotropic MP nanocomposites (G and J) can be produced through a post–modification approach.

notable one is the one–pot approach, enabling the simultaneous in situ growth of multiple plasmonic and magnetic components.[52] This method is beneficial for environmental preservation and cost efficiency, as it minimizes chemical consumption and reduces harmful waste generation. Typically, this process is executed through a chemical reduction approach, where selecting the right solvent and reducing/stabilizing agents is crucial for the proper synthesis of both components. For instance, Fan et al. (2016) successfully utilized this method to synthesize Ag–Fe_3O_4 nanocomposites, employing them as efficient SERS substrates.[53] They conducted the reduction and growth of silver and iron precursors in an aqueous solution with polyvinyl pyrrolidone (PVP) at 90 °C, yielding spherical iron oxide NPs adorned with small silver NPs. Despite a non–uniform NP distribution, there was a notable red shift in the absorption peaks due to the incorporation of both components, enhancing SERS activity. Guardia et al. (2017) reported a similar synthesis of monodisperse Au–Fe_3O_4 dimers via a one-pot approach, but in an organic solvent (1-octadecene) with oleic acid and oleylamine, allowing the reduction and growth of both precursors at elevated temperatures.[54] Furthermore, this approach can facilitate the growth of one–dimensional nanocomposites, such as nanowires, by employing suitable polyols for elongated growth through specific crystalline facets.[55]

In producing MP nanocomposites, several factors must be considered. The precursor NPs need compatible properties for optimal nanocomposite characteristics. Four main approaches are commonly employed: chemical bonding–based fabrication, physical mixing-based production, self–assembly, and coating methods.

Chemical bonding–based fabrication involves uniting diverse materials through chemical interactions.[56] This method starts with the separate preparation of magnetic and plasmonic NP components, focusing on dimensions, shapes, and surface attributes. Functional groups or ligands, like sulfhydryl (–SH), amino (–NH2), or carboxyl (–COOH) moieties, are then selected to establish robust chemical bonds with NP surfaces. For example, a study coated Fe_3O_4 NPs with functionalized SiO_2 having $–NH_2$ groups, onto which Au NPs were deposited.[57] Physical mixing-based fabrication is a simpler technique that merges materials through physical blending.[58] This method combines magnetic and plasmonic NPs by agitation or stirring in a suitable solvent, leading to a random distribution and influencing the nanocomposite's physical properties.[8b,59] Self–assembly utilizes the spontaneous organization of materials based on molecular–scale interactions.[60] In this method, magnetic and plasmonic components with modified surfaces are placed in a solvent. Their self–organization is driven by forces like electrostatic attractions or hydrogen bonds. For example, Wang et al. (2019) used DNA origami to combine magnetic ring–like structures with plasmonic NPs, achieving designs beyond conventional colloidal self–assembly (Figure 4).[61] The coating method involves applying a layer of one material onto another.[62] This solution–based process applies a plasmonic precursor onto the surface of magnetic NPs, forming

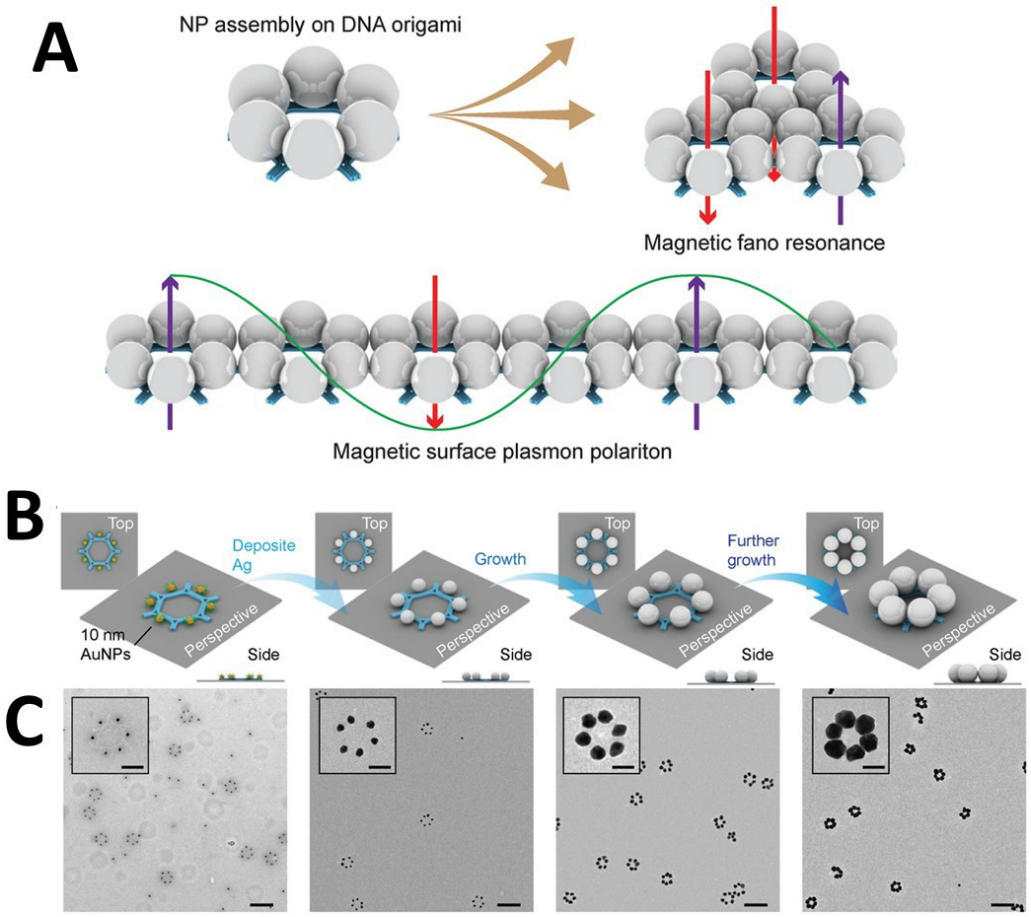

Figure 4. A) An illustrative diagram depicts intricate magnetic plasmon NP networks meticulously assembled on DNA templates. It showcases a hexagonal NP ring meticulously arranged on a DNA origami structure. The programmable assembly of DNA origami results in the creation of intricate magnetic plasmon architectures, including magnetic surface plasmon polaritons B) Schematic diagrams and C) transmission electron microscopy (TEM) images are presented for magnetic rings, which were fabricated through a sequential growth process involving Ag NPs. The scale bars in the images are 200 nm, with insets showing a higher magnification view at 50 nm. Adapted with permission from ref. [61] Copyright 2019 John Wiley and Sons.

a homogeneous layer. The shape of the plasmonic shell can be manipulated to enhance SERS signals, as in the case of star–shaped anisotropic morphologies.[63] Laser–assisted synthesis is an innovative approach, creating homogeneous noble metal–transition metal nanoalloys at the single NP level.[64] This method uses laser ablation in a liquid solution to generate metal ions and clusters from metal targets, facilitating alloying and nucleation. Amendola et al. (2014) and Mohan et al. (2017) explored this approach for synthesizing Au–Fe and AuFePt ternary alloy structures, respectively, demonstrating the influence of composition on plasmonic properties and SERS performance.[65,66]

3. Magnetic–Plasmonic Nanocomposites in SERS-Based Applications

MP nanocomposites are integral to advancements in SERS based applications. These nanocomposites, created by amalgamating magnetic and plasmonic components, provide an effective substrate for amplifying SERS signals of target analytes. The magnetic component of these nanocomposites enables precise targeting and manipulation of the sample in a specific area,[3b] while the plasmonic component is crucial for enhancing Raman signals by concentrating electromagnetic fields on its surface. As a result, MP nanocomposites have emerged as sensitive and powerful analytical tools in SERS spectroscopy, with widespread applications spanning biomedicine, environmental analysis, and materials science. In a broader context, MP SERS substrates can be categorized into four main types, each distinguished by their unique compositions, functionalities, and application areas. These categories reflect the diverse ways in which magnetic and plasmonic properties can be combined and tailored to meet specific analytical needs in various fields. Understanding these categories provides insight into the versatility and potential of MP nanocomposites in enhancing the sensitivity and specificity of SERS-based detection methods.

3.1. Magnetic–Plasmonic Core–Shell Nanocomposites

Core–shell MP nanocomposites are commonly utilized in various SERS-based applications,[67] with the plasmonic shell coating on magnetic nanoparticles enhancing their biocompatibility and broadening their use in biological contexts.[68] The magnetic and plasmonic properties of these nanocomposites can be finely tuned by adjusting the shell thickness, core/shell morphology, or the proportion of core and shell components. This tunability is crucial in SERS applications since slight changes in core–shell composition can significantly impact the magnetic and plasmonic responses. In some cases, the core may not necessarily be magnetic but plasmonic, with a subsequent magnetic shell coating, potentially followed by a second plasmonic shell to form a (core@shell)@shell structure (Figure 5A). When organized under an external magnetic field, these simple yet effective plasmonic structures become highly suitable for SERS applications (Figure 5B). The SERS performance of core–shell MP nanocomposites is notably influenced by the thickness of the plasmonic shell on the magnetic core.[69] Altering the shell thickness can significantly affect the SERS enhancement factor (EF), but this relationship is not always linear. For example, a study showed that the optimal SERS performance for Ni : Au ratio core–shell substrates was achieved

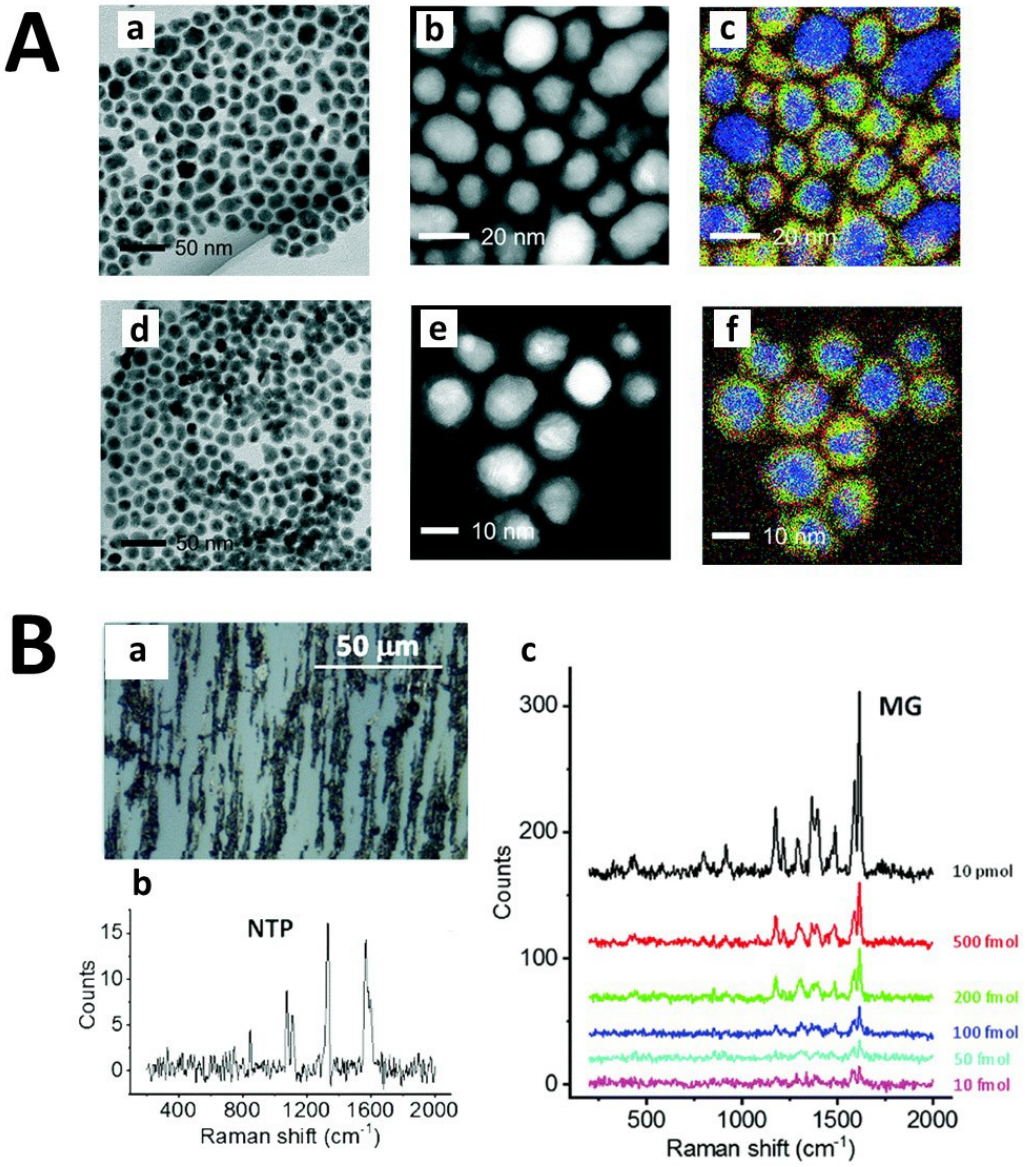

Figure 5. A) TEM images of (a) Ag@FeCo and (d) Ag@FeCo@Ag NPs, scanning transmission electron microscopy–high angle annular dark field (STEM–HAADF) images of (b) Ag@FeCo and (e) Ag@FeCo@Ag NPs, and energy–dispersive X-ray spectroscopy (EDS) elemental mapping images of (c) Ag@FeCo and (f) Ag@FeCo@Ag NPs. Blue, red, and green lines corresponding to the Ag, Fe, Co, respectively. Adapted with permission from ref.[140] Copyright 2015 Royal Society of Chemistry. B) Optical microscope image (a) of Fe@Au NPs deposited on a microscope glass slide in the presence of an external magnetic field, (b) Raman spectrum obtained with 532 nm excitation of Fe@Au NPs coated with nitrothiophenol (NTP), displaying characteristic peaks associated with the ligand, and (c) Raman spectra recorded after drop–casting malachite green (MG) onto Fe@Au NPs at various concentrations. This approach enables the detection of the analyte at concentrations as low as 10 fmol added to the substrate. Adapted with permission from ref.[141] Copyright 2019 Royal Society of Chemistry.

at 50:50, with deviations from this ratio leading to reduced performance.[67a] The ferromagnetic properties of the nickel core were found to impact the surface electrons, affecting the SERS signal.

The choice of magnetic and plasmonic materials, as well as the nanocomposite's morphology, is critical in determining SERS response. For instance, Yang et al. (2017) compared branched and smooth gold–coated magnetic nanocomposite substrates (B-GMNP and S-GMNP, respectively) with a Fe_3O_4@SiO_2@Au composition for detecting mitochondrial RNA-21 (miRNA-21). They found that B-GMNPs, with their tip–enhancement effect, were more sensitive than S-GMNPs.[70] Additionally, the superparamagnetic property of the Fe_3O_4 core allowed for controlled separation and enrichment.[71]

The morphology of the magnetic material forming the core can also significantly impact the properties of the core–shell nanocomposite. Levin et al. illustrated this with their study of nanocomposites with a faceted or tetracubic wüstite (Fe_xO) nanocrystal core (Figure 6).[72] They observed that the magnetic properties were preserved, with changes in the plasmonic nature of the nanocomposite due to the core's high dielectric constant. Such designs, compared to traditional magnetic cores, can achieve more regular geometries and avoid aggregation during plasmonic shell coating.[73] Furthermore, certain core morphologies, like cubic ones, provide more surface area and sharp vertices, enhancing the SERS effect.[74]

3.2. Magnetic–Plasmonic Core–Satellite Nanocomposites

Core–satellite MP nanocomposites, distinct from core–shell materials, feature a configuration where plasmonic nanoparticles (NPs), smaller than the core or template, are dispersed on its surface rather than forming a continuous shell. This arrangement creates a high density of electromagnetic 'hot-spots' due to the proximity of these particles. Such nanocomposites, often comprising gold on a silver core or the reverse, have been extensively fabricated and are recognized for their effectiveness in various SERS-based applications.[75]

The collaboration of different plasmonic materials in these nanocomposites results in robust substrates capable of detecting analytes at ultra–low concentrations. The specific morphology of the nanocomposite elements plays a vital role in this process.[76] Another interesting variation of core–satellite nanocomposites involves structures where the core consists of magnetic NPs with plasmonic NPs attached, either through electrostatic or covalent bonding.[77] The larger size of the magnetic core compared to the satellite NPs is a key factor in these designs. If a plasmonic material forms the core, the dimensions may exceed the wavelength of light, transitioning from localized surface plasmon resonance (LSPR) to surface plasmon resonance (SPR) and potentially diminishing the plasmonic properties.

In MP substrates designed for SERS applications, the material constituting the magnetic part is often less critical than achieving a substrate that combines magnetic manipulability with strong plasmonic effects. Moreover, core–satellite MP nanocomposites can be constructed not only from a single core but also by combining multiple cores with magnetic properties. This approach allows for the creation of a morphology that imparts greater maneuverability to the nanocomposite. An example of this is the work by Wang et al. (2020), where Fe_3O_4 NPs were initially assembled via a self–assembly protocol and then enriched with Ag NPs after a SiO_2 coating.[78] This MP nanocomposite, under an external magnetic field, exhibits rotational motion within the solution, increasing interactions with the target analyte and facilitating SERS-based detection (Figure 7).

3.3. Anisotropic Magnetic–Plasmonic Nanocomposites

Anisotropic MP nanocomposites can be fabricated using two fundamental methods: (i) creating a magnetic core with an anisotropic morphology and then coating it with a plasmonic shell,[79] or (ii) inducing anisotropy in the plasmonic shell through post–modifications.[80] The resulting anisotropic morphology, characterized by a lack of symmetry, allows for the focusing of the electromagnetic field onto specific points on the plasmonic surface, thereby enhancing SERS signals.

The most commonly encountered anisotropic morphology in MP nanocomposites is the star–shaped structure.[81] This morphology enables the accumulation of a high electromagnetic field at the tips of its elongated branches. The primary distinction between star–shaped and spherical plasmonic nanocomposites lies in the tunability of the localized surface plasmon resonance (LSPR) as the nanocomposite's tip sizes change. Unlike spherical nanocomposites, which typically require proximity to each other to form hot–spots, star–shaped MPs can independently enhance the electromagnetic field in isolation. Due to their strong SERS capabilities, star–shaped MPs are preferred in many studies, despite the need for sophisticated production techniques.

A common method for fabricating star–shaped MP nanocomposites involves transforming a spherical core–shell structure into a star–shaped morphology. For example, in the study by Tomitaka et al. (2020), the magnetic core was initially synthesized using the co–precipitation method.[82] This core was then functionalized with citrate and coated with a gold shell, which was subsequently transformed into a star–shaped morphology using ascorbic acid and $AgNO_3$. Alternatively, star–shaped MP nanocomposites can be created by initially synthesizing a plasmonic core and then coating it with magnetic nanoparticles. Muzzi et al. (2022) demonstrated this approach by producing oleylamine–capped Au nanoparticles and using oleylamine as a nucleation center for Fe_3O_4, forming MP nanocomposites with a star–shaped morphology.[83] In such structures, the thick, homogeneous coating of the plasmonic core with a magnetic material allows for more precise control of the plasmonic resonance energy,[84] often resulting in a more pronounced redshift compared to classical magnetic@plasmonic nanocomposites.

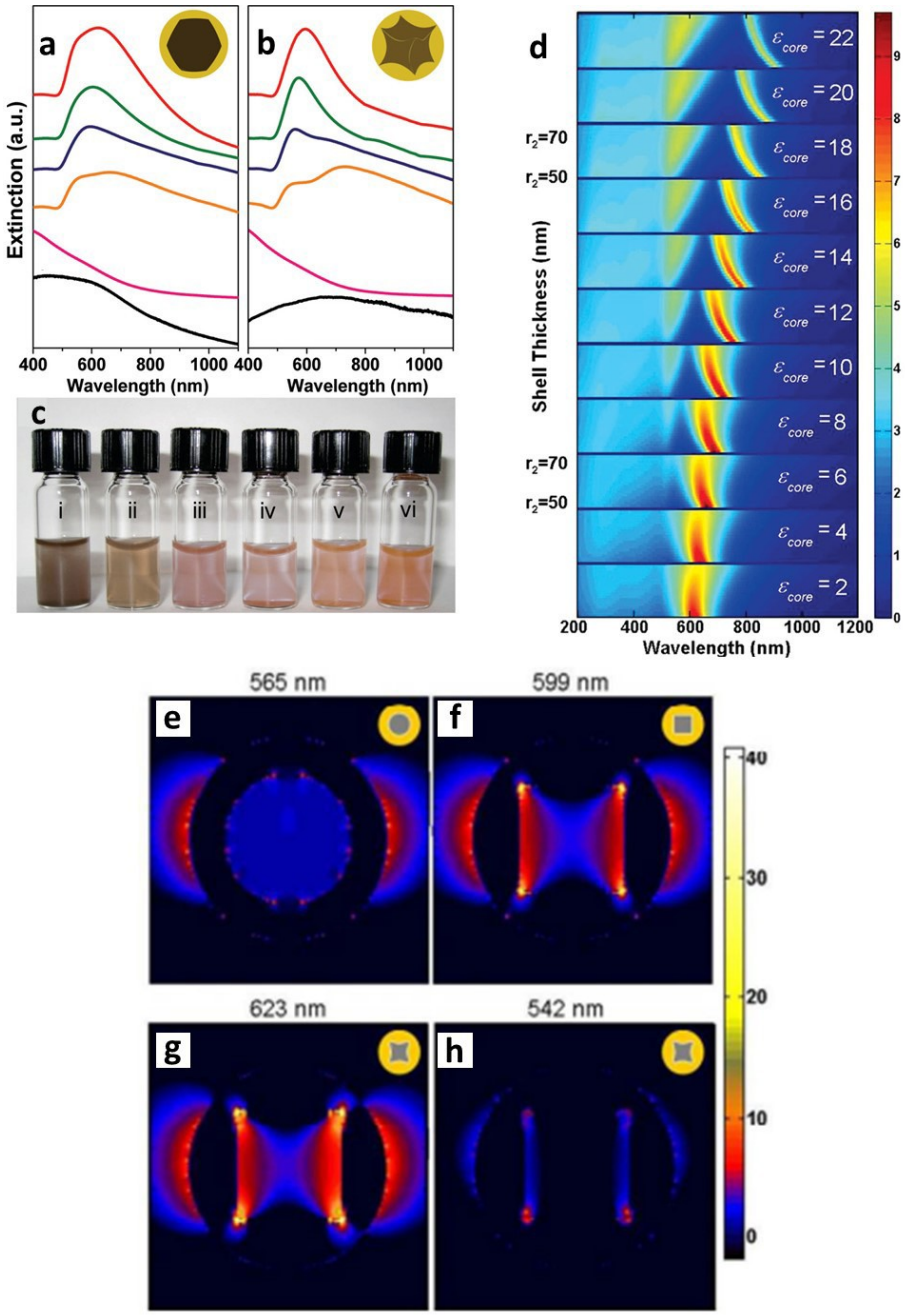

Figure 6. The magnetic and plasmonic properties of the nanocomposite can be precisely tuned by adjusting the thickness of shell, morphology of core/shell or proportion of the core and shell components individually: Solution extinction measurements were conducted for (a) faceted and (b) tetracubic Au–coated Fe_3O_4 NPs under various conditions. The black colour represents the uncoated cores in the spectra. It is evident from the upward trend that increasing plasmonic shell thickness from bottom to top significantly alters the optical properties of the particles. (c) displays an optical image of the particles shown in (a). (i) represents an uncoated magnetic core. From (ii) to (vi) depict increasing shell thickness. A theoretical colour contour (d) representation is presented, depicting the extinction spectra for various core dielectric permittivities and shell thicknesses, all with an identical effective core radius ($r_{eff} = r_1 = 36$ nm). Each panel showcases the extinction spectra for a constant ε_{core}, while the shell radius increases from $r_2 = 50$ nm to $r_2 = 70$ nm. The colour scale corresponds to the normalized extinction cross–section values relative to the maximum extinction value. A comparison of the electric field enhancement distribution in an equatorial plane passing through the centre of three different shells. Specifically, the dipolar modes ($l = 1$) are depicted for (e) a spherical core at 565 nm, (f) a cubic core at 599 nm, and (g) a concave cubic core at 623 nm. Furthermore, (h) showcases the quadrupole mode ($l = 2$) for the concave cubic core geometry at 542 nm. Adapted with permission from ref.[72] Copyright 2009 American Chemical Society.

3.4. Janus–Type Magnetic–Plasmonic Nanocomposites

Janus particles exhibit distinct surface properties on their opposite sides, offering asymmetric morphology at the nano- and micro–scale. Janus particles can incorporate materials with different physical, chemical, and mechanical properties within a single particle, resulting in a synergistic amplification effect.[85] Depending on the application, Janus particles may be com-

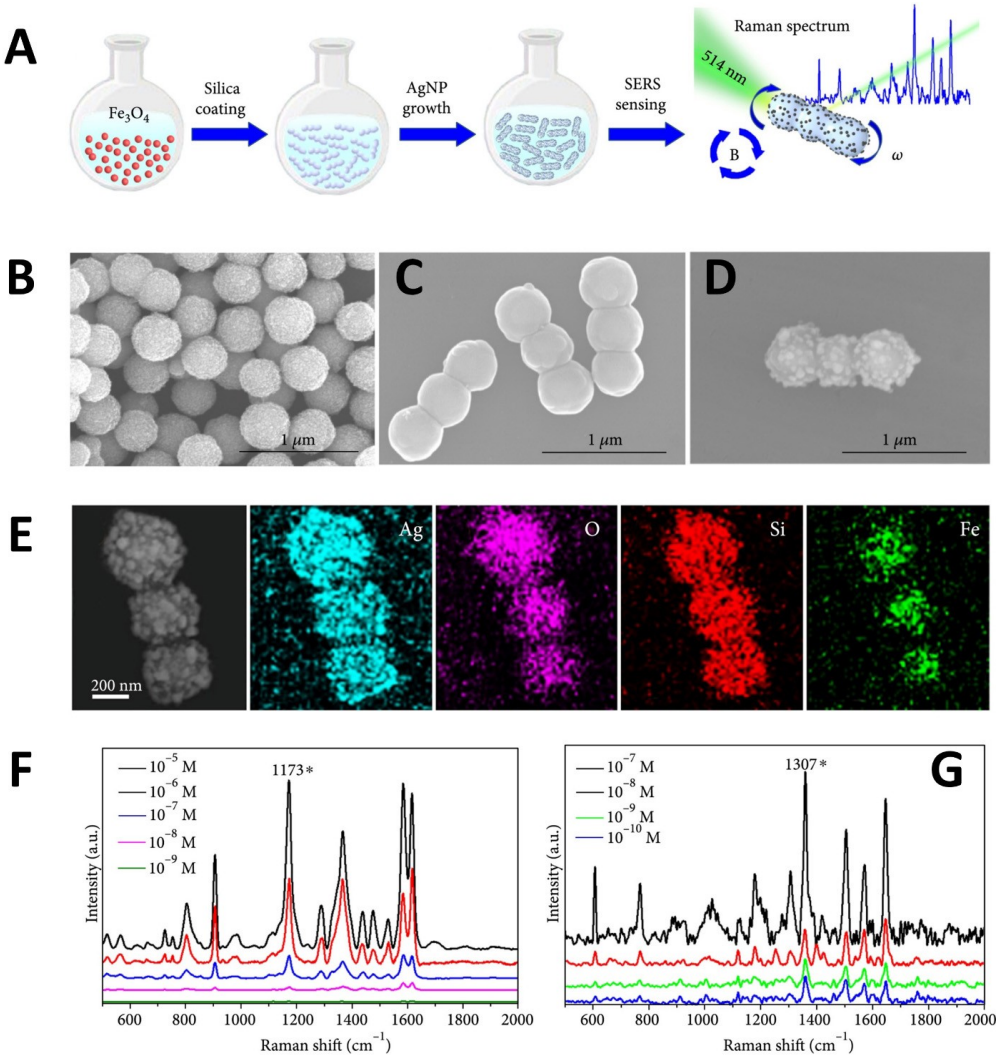

Figure 7. A) A schematic illustration depicting the fabrication process and SERS-based sensing application of the magnetic NR-Metallic Ag Particle system. SEM images of B) Fe_3O_4 NPs, C) silica (SiO_2)–coated magnetic NRs, and D) magnetic rod decorated with Ag NPs, respectively. E) EDS elemental mapping of rod–like magnetic SERS probes, and SERS spectra of different concentrations of F) crystal violet (CV) and G) R6G, respectively. Adapted with permission from ref.[142] Copyright 2020 American Association for the Advancement of Science.

posed of entirely organic combinations, organic–inorganic hybrids, or entirely inorganic combinations, with morphologies tailored to specific requirements (Figure 8A).[86]

Janus–type nanocomposites with magnetic properties have gained attention not only for their combination with plasmonic metals but also for their integration with various other materials.[86] These nanocomposites exhibit synchronized self–assembly properties,[87] aiming to achieve complex and multi-scale organization through magnetic field–directed colloidal assembly (Figure 8B, C).[88] This capability enables the creation of sophisticated structures using magnetic Janus particles.

In terms of MP nanocomposite properties, the directed self–assembly feature with an external force is particularly useful. This assembly enhances the electromagnetic field due to the strong coupling of the plasmonic parts of the particles and the formation of hot–spots. Additionally, Janus particles' self–assembly properties can be influenced by surface agents like amphiphilic polymers, organizing MP Janus nanocomposites into vesicular superstructures in a medium, thus enhancing electromagnetic and magnetic properties. For example, Au–Fe_3O_4 Janus–type nanocomposites functionalized with hydrophilic polyethylene glycol (PEG) and hydrophobic polystyrene (PS) exhibit different vesicular structures depending on the grafted polymer part[90] (Figure 8D).[89] This modification can increase the SERS enhancement factor for probes like thiolated Rhodamine (RhB–SH). Other studies have shown that Janus–type MP nanocomposites can self–assemble based on hydrophilic/hydrophobic behavior or through pH-triggered mechanisms enabled by pH-sensitive polymers,[90] enhancing their utility in SERS spectroscopy and related applications.

When using Janus–type MP nanocomposites in SERS applications, the surface area of the magnetic and plasmonic lobes is crucial. For instance, dumbbell–like MP Janus-type nanocomposites may have limitations due to the small area occupied by the plasmonic portion, resulting in weak LSPR bands.[91] Therefore, the plasmonic portion should ideally be

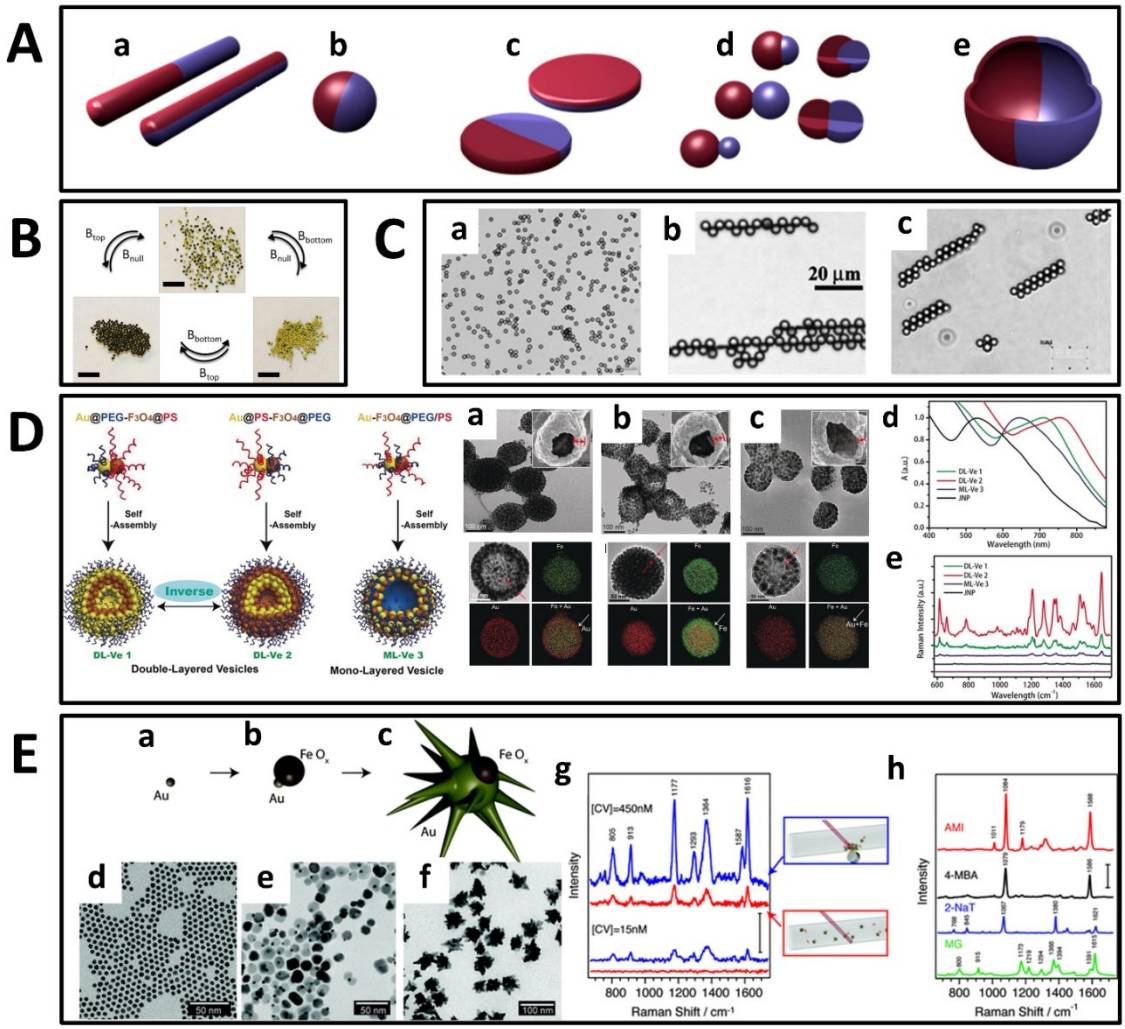

Figure 8. A) Janus–type particles in different types: a) Cylindrical, b) Spherical, b) Disc–shaped, d) Different types of dumbbell–shaped Janus particles with symmetric or asymmetric character, e) Janus vesicles or capsules. Adapted with permission from ref.[143] Copyright 2013 American Chemical Society. B) Magnetic Janus–type particles (Top) randomly distributed in the absence of magnets (B_{null}). If the magnet is applied from the top (B_{top}) or the bottom (B_{bottom}), the particles are rearranged according to the location of the magnet. Black colour indicates the magnetic lobe in the spherical Janus–type particle. Adapted with permission from ref.[144] Copyright 2020 John Wiley and Sons. C) Besides being aggregated in the presence of magnets, magnetic Janus-type particles can also be arranged in certain ways: a) Before magnetic field is applied, b) Staggered and c) Double chain self–assemblies obtained when ~0.15 T magnetic field is applied. Adapted with permission from ref.[145] Copyright 2009 Royal Society of Chemistry. D) Schematic illustration of the Janus–type Au–Fe_3O_4 MP nanocomposites grafted with the polymers, and the hierarchical self–assembly of the resulting three kinds of Janus–type amphiphilic nanocomposites into double–layered MP vesicle 1 and 2 and mono–layered vesicle 3 in aqueous media: a–c) TEM, SEM images, and TEM-element mapping images of the DL–Ve 1, DL–Ve 2, and ML–Ve 3, d) UV-vis spectra of the Janus–type MP nanocomposites and self-assemble structures and, e) SERS spectra of the materials. Adapted with permission from ref.[89] Copyright 2017 John Wiley and Sons. E) Schematic representation of the preparation of Janus–type MP nanocomposites: a) Au NPs, b) Growth of an iron oxide NP through the decomposition of $Fe(CO_5)$ and subsequent oxidation, c) Growth of an Au NS coated with poly (vinylpyrrolidone) (PVP) using the NDs as seeds, d–f) TEM images of different NPs corresponding to the scheme above, g) SERS spectra of CV containing the materials in solution (red) and after magnetic concentration (blue) for two different dye concentrations [CV] = 450 nM (upper spectra) and [CV] = 15 nM (lower spectra), and (h) SERS spectra of different molecules after a magnetic aggregation. AMI: Acetoamidothiophenol, 4-MBA: 4-Mercaptobenzoic acid, 2-NAT: 2-Naphthalenethiol. Adapted with permission from ref.[92] Copyright 2016 Royal Society of Chemistry.

larger than the magnetic portion and, if possible, have an anisotropic morphology for SERS applications. Reguera et al. (2016) addressed this by transforming the plasmonic portion of nanodumbbell Janus–type MP nanocomposites into a larger, star–shaped morphology (Figure 8E).[92] This modification led to a stronger LSPR band and a red–shift in UV-vis absorbance, making these nanocomposites ideal for biological SERS applications. Additionally, under a magnetic field, particle aggregation occurred, leading to a higher SERS signal for low concentrations of analytes like crystal violet (CV), demonstrating the potential of Janus–type MP nanocomposites in SERS-based applications.

3.5. Magnetic–Plasmonic Nanoalloys

Plasmonic nanoalloys represent a distinct and promising class of materials in the field of SERS substrates, differing fundamentally from heterostructures. These nanoalloys are created by amalgamating two or more different elements, resulting in a

multifunctional structure within a single entity. A particularly appealing strategy in SERS applications involves introducing magnetic properties into these nanoalloys by alloying plasmonic materials with magnetic elements such as Fe, Ni, or Co. This approach endows the nanoparticles (NPs) with novel physico–chemical properties and the ability to be precisely controlled under a magnetic field, thereby enhancing their effectiveness in SERS-related technologies. The incorporation of magnetic properties into nanoalloys has been demonstrated to significantly amplify the plasmon–induced local electromagnetic (EM) field when NPs accumulate in a specific region, facilitated by an external magnetic field.[93] This enhancement leads to improved overall performance in SERS applications. Various nanoalloy structures, such as Au/Fe, Au/Co or Ag/Fe,[94] have been developed and documented as highly efficient magneto–plasmonic substrates. These structures have shown remarkable SERS performance, exemplifying the potential of combining multiple functionalities within a single, unified framework.

4. The Surface Functionalization of Magnetic–Plasmonic Nanocomposites

4.1. Silica

The SiO_2 coating procedure for various nanomaterials is primarily undertaken for several reasons: (1) to ensure stability, (2) to create a larger surface area for surface modification, or (3) to enhance protection. From a SERS perspective, the SiO_2 shell prevents direct contact of the Raman–active molecules with the external environment, thus maximizing the SERS performance of the resulting nanocomposites. In a study, Fe_3O_4/Ag MP nanocomposites were first functionalized with 2-mercaptoethanesulfonate (MES) before growing SiO_2 shells on them (Figure 9A). The findings showed that the SiO_2 shell acted as a robust barrier against harsh external factors, maintaining the stability of the SERS signal from the Raman molecule. It was also emphasized that the presence of the SiO_2 shell led to a more homogeneous distribution of the MP nanocomposites, particularly under magnetic assembly conditions.[95]

Furthermore, the SiO_2 shell not only protects MP nanocomposites from the external environment but also acts as a barrier that shields biological environments from potentially toxic nanocomposites. For example, when MP nanocomposites contain a plasmonic component like Ag, SiO_2 can serve as a barrier to prevent the release of Ag^+ ions, which could induce toxicity in various cell lines. Sotiriou et al. (2011) produced Ag/Fe_2O_3 Janus MP nanocomposites coated with SiO_2 to assess their cytotoxic effects on Raji and HeLa cells.[96] The study demonstrated that the SiO_2 coating significantly reduced the release of Ag+ ions from the nanocomposites, minimizing flocculation and agglomeration in the cell environment compared to uncoated ones. Another significant advantage of the SiO_2 shell is its ability to provide a high surface area for various plasmonic nanoparticles or layers. For instance, Liu et al. (2023) fabricated Fe_3O_4@SiO_2@Au MP nanocomposites and, using 4-mercaptopyridine (4-MPy), conducted indirect detection of Hg^{2+} metal ions in water.[97] The primary objective was to protect the magnetic core from oxidation and provide ample surface area for the plasmonic component of the nanocomposite, facilitated by the SiO_2 shell. The results enabled the detection of Hg^{2+} ions at parts–per–billion levels (Figure 9B). In another study, flower–shaped MP nanocomposites were used for the detection of a gold-standard biomarker for acute myocardial infarction, cardiac troponin I (cTnI).[98] The process began with the synthesis of magnetic Fe_3O_4, followed by SiO_2 coating. Subsequently, branched Ag nanoparticles were positioned on this supporting shell, enabling detection of cTnI at femtogram levels.

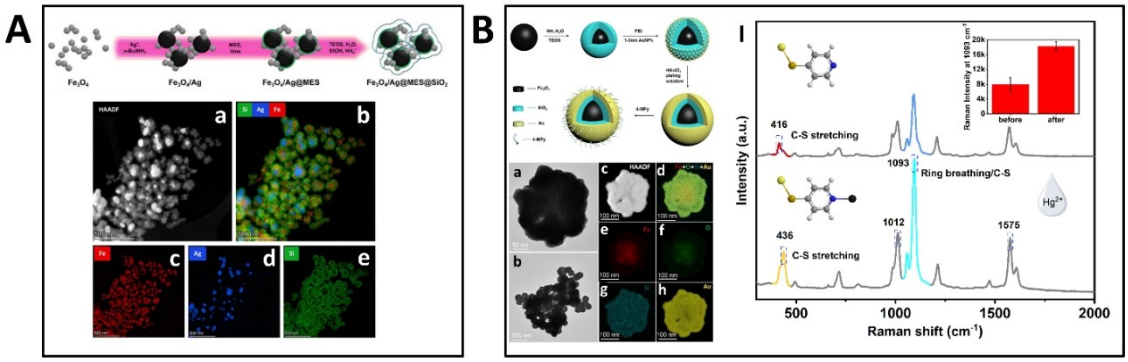

Figure 9. A) Schematic illustration of the preparation of Fe_3O_4/Ag@MES@SiO_2 nanocomposite: (a) STEM–HAADF and corresponding (b–e) STEM–EDX elemental mapping images showing the distribution of respectively overlay of Fe + Ag + Si and individual Fe, Ag and Si. Adapted with permission from ref.[95] Copyright 2021 Frontiers. B) Synthesis route of Fe_3O_4@SiO_2@Au/4-MPy composite microspheres: (a–b) TEM images, (c) bright-field TEM image and (d–h) corresponding elemental mapping of the composites. (I) The SERS spectra of Fe_3O_4@SiO_2@Au/4-MPy composites before and after adding Hg^{2+} ions (10 ppm). Inserted image is the corresponding SERS intensities of 4-MPy at 1093 cm^{-1}. Adapted with permission from ref.[97] Copyright 2023 Molecular Diversity Preservation International.

4.2. Polymers

The primary goal of incorporating a polymer–coated MP (magnetic–plasmonic) nanocomposite is to provide mechanical support and introduce functional side groups, the nature of which depends on the type of polymer used.[98] Similar to the SiO_2 example, other objectives include ensuring the nanocomposite's stability within its environment and providing protection. Polymers in MP nanocomposites can be utilized in two main ways. Firstly, functionalizing the magnetic core with a specific polymer can effectively protect the core from oxidation, reduce the generation of toxic free radicals, and aid in enlarging the plasmonic shell. This role of the polymer is often referred to as the 'glue'.[99] It's crucial that the polymer serving as the glue meets certain criteria, including biocompatibility and having necessary metal–binding regions for forming the plasmonic shell. However, it's important to note that not every polymer is suitable for this role, and the choice of polymer can significantly affect the SERS performance of the MP nanocomposites. For example, a study by Sirgedaite et al. (2022) explored different polymeric glues like polyethyleneimine (PEI), polyvinyl alcohol (PVA), and PEG for decorating magnetite nanoparticles with Au and Ag nanoparticles.[100] The study found that magnetite nanoparticles coated with PEI, due to its positive charge, showed a greater affinity for plasmonic nanoparticles, leading to higher SERS intensities for the 4-mercaptobenzoic acid (4-MBA).

In addition to using polymers as a 'glue' in MP nanocomposites, another approach is to coat the entire nanocomposite with suitable polymers to achieve specific applications. This coating enables the nanocomposite to acquire functional groups such as –COOH, $–NH_2$, –OH, and –SH. These moieties enhance the SERS response by capturing various molecules. In some cases, the electrostatic interaction between the analyte and the polymer alone can be sufficient for strong SERS detection. For instance, a study by Pinheiro et al. (2019) demonstrated this by coating MP nanocomposites with PEI for the SERS detection of tetracycline (TC), an antibiotic.[101] The strong electrostatic interaction between the negatively charged TC molecules and the positively charged PEI facilitated separation from the aqueous phase, achieving a detection limit as low as 10 nM. Moreover, polymer coating not only functionalizes the surface but can also impart hydrophilic or hydrophobic properties to the nanocomposite, depending on the polymer type. De la Encarnación et al. (2022) illustrated this in their production of MP nanocomposites for MRI, SERS, and fluorescent imaging (FI).[102] They synthesized spherical magnetic cores, deposited Au nanoparticles on them, and transformed these plasmonic nanoparticles into spiky shells. The resultant MP nanocomposites were then coated with an amphiphilic polymer, polyisobutylene–alt–maleic anhydride (PMA), rendering them hydrophilic and highly dispersible in water, ideal for biological applications. The authors also noted that PMA-coated nanocomposites could be easily functionalized with fluorescent dyes like carboxytetramethylrhodamine (TAMRA) and DY633.

4.3. Biological species

Biological molecules represent another agent utilized in the surface functionalization of MP (magnetic–plasmonic) nanocomposites.[103] This type of functionalization is especially relevant in medical applications.[104] A notable example is the work of Zou et al. (2015), who engineered a complex composed of Fe_3O_4, Au, and graphene quantum dots (QDs). This complex was functionalized with G2 and G3 antibodies for the simultaneous detection of the CFP-10 antigen, a marker in tuberculosis, using both fluorescence and SERS (Surface–Enhanced Raman Scattering)–based methods.[105] A critical aspect of this approach is the external application of a magnetic field, which aligns the MP nanocomposites into one-dimensional (1D) structures, forming organized nanowires (NWs). This alignment not only amplifies the SERS effect but also enhances the metal-enhanced fluorescence (MEF) effect, leading to strong fluorescence exhibited by the graphene QDs. As a result, the authors achieved successful detection of the CFP-10 antigen down to a concentration of 0.0511 pg/mL.

Another significant advantage of functionalizing MP nanocomposites with biological agents is their capability to bind similar or different types of nanocomposites together. This property is crucial for creating bilayer or 'sandwich-type' SERS sensors, which are increasingly popular in medical applications due to their high–precision results.[106] An intriguing example of this application is found in the study by Zhao et al. (2022).[107] In their research, the team initially created core–satellite type MP nanocomposites by decorating an Fe_3O_4 core with Au nanoparticles, facilitating magnetic separation. The surface of these Au nanoparticles was then functionalized with double–stranded DNA (dsDNA). By integrating the functionalized Au nanospheres with 4-MBA and another DNA strand through DNA hybridization, they successfully detected the antibiotic tobramycin at an exceptionally low level of 0.44 fg/mL. This showcases the remarkable sensitivity and specificity that can be achieved through the strategic functionalization of MP nanocomposites with biological agents.

4.4. Sieving Materials

The term 'sieving materials' typically refers to porous materials used as a sieve or filter to separate or extract molecules of specific sizes. In SERS applications, coating MP nanocomposites with such materials can effectively reduce background signals, a common challenge in complex environments. Additionally, precise control over the pore size and openings of the sieving material allows targeted analytes to selectively pass through and reach the plasmonic surface, enhancing SERS sensitivity. Porous silica ($pSiO_2$) is a commonly encountered sieving material in SERS applications.[108] Its widespread use is largely due to its ability to isolate MP nanocomposites from the surrounding environment, ensuring consistent performance. Moreover, $pSiO_2$'s porous nature allows for the deposition of additional plasmonic structures, significantly enhancing SERS. For example, Wang et al. (2023) utilized $pSiO_2$ in fabricating

sandwich-type MP nanocomposites for detecting *Staphylococcus aureus*.[109] They synthesized dendritic mesoporous SiO_2 nanoparticles (DMSN), filled them with Au@Ag nanoparticles, and functionalized them with concanavalin A specific to the bacterium. Additionally, they functionalized Fe_3O_4@Au nanoparticles with antibodies to create the nanocomposite, achieving a detection limit of 7 CFU mL^{-1}.

While $pSiO_2$ is essential in SERS applications, it's not without drawbacks. The primary challenge lies in precisely controlling its pore size, morphology, and volume.[110] Its synthesis often requires calcination at high temperatures, which can decrease magnetic properties in structures containing magnetic components like MP nanocomposites. Although $pSiO_2$ can achieve high surface areas ($\approx$1500–2000 $m^2 g^{-1}$),[111] most such materials are mesoporous and lack dynamic pore structures. Thus, there is a need for materials with more dynamic host/guest relationships, finely tuneable porosity, and higher surface areas in SERS applications. Metal–organic frameworks (MOFs) and covalent–organic frameworks (COFs) have emerged as significant alternatives in this context.

MOFs are known for their robust bonds between polynuclear metal clusters and organic 'linkers', forming well–defined crystalline lattice structures. The diversity of metal ions and organic linkers allows for the synthesis of frameworks with varied properties and complexity levels, making MOFs ideal for SERS applications.[3a] In contrast, COFs, composed entirely of organic building blocks, offer lightweight properties and environmental stability due to the covalent bonds in their structure. However, COF research, especially in combination with MP nanocomposites for SERS, is still in its infancy. A study by Bölükbaşi et al. (2022) exemplifies this, where they coated Fe_3O_4 nanoparticles with imine–linked COFs composed of 1,3,5-tris(4-aminophenyl) benzene (TAPB) and 2,5-dimethoxyterephthaldehyde (DMTP) building blocks, and decorated them with Au nanoparticles for electrochemical sensing.[112] Another study by Yang et al. (2022) involved synthesizing imine–linked COF particles with DMTP and TAPB, growing Au nanoparticles in situ, and functionalizing with concanavalin A to create sandwich–type sensors for detecting bacteria like *Escherichia coli* and *Salmonella enteritidis*.[113]

MOFs are often preferred over COFs due to their well–documented properties. COF research, primarily focused on imine–linked COFs, faces challenges such as particle size control and lengthy, solvent-dependent synthesis processes.[114] In contrast, MOFs' suitability for extracting and separating molecules has been demonstrated in various studies.[115] Lai et al. (2019) decorated Fe_3O_4 nanoparticles with Au and coated them with MIL-100(Fe) MOF, successfully extracting and detecting MG and thiram with detection limits of 4.4 nM and 15 nM, respectively.[116] Sun et al. (2022) produced Fe_3O_4@UiO-66-NH_2@Au nanocomposites for isolating the thiabendazole fungicide, achieving a detection limit of 6.5 ppb (Figure 10A).[117] Ge et al. (2023) coated magnetic prickly–like nickel nanorods with MOF-74(Ni) and enriched them with Ag nanoparticles, detecting mycotoxins T-2 and deoxynivalenol (DON, Figure 10B).[118] These studies highlight the role of MOFs as novel and effective sieving materials in SERS applications, enabling the isolation of various analytes by MP nanocomposites.

5. SERS-Based Applications of Magnetic–Plasmonic Nanocomposites

5.1. Separation

Separation applications of MP nanocomposites are critically important in the field of SERS, particularly for the selective separation of analytes from complex media.[67d,107] The magnetic cores in these nanocomposites facilitate rapid binding of analytes, enabling easy removal from solutions and preparation for SERS analysis. This is particularly crucial in diagnosing analytes that require molecular–level monitoring. For example, Zhang et al. (2022) developed a magnetic fluid–based microfluidic chip decorated with Ag nanoparticles for MG detection in point-of-care (POC) testing.[119] The study highlighted the effective isolation of MG by the nanocomposites, allowing for SERS detection at the picomolar level.

In some instances, intermediate layers are used to expedite the separation process and direct the target molecule towards the MP nanocomposites. One study employed Fe_3O_4 nanoparticles coated with ZrO_2 and decorated with Ag nanoparticles for the SERS detection of hexavalent chromium (Cr(VI)) (Figure 11A).[120] The ZrO_2 layer functioned as an adsorbent, selectively adsorbing Cr(VI) through Zr–O coordination bonds, thus facilitating its isolation for low–concentration SERS detection (10^{-7} M). Intermediate layers also enable the development of more sophisticated morphologies in MP nanocomposites. Zou et al. (2022) produced nanocomposites with magnetic cores and Au spikes.[121] They modified Fe_3O_4@SiO_2 particles with $AgNO_3$ and PVP, creating an intermediate layer that was further treated with $HAuCl_4$ and Dopa. The formation of a Dopa-Ag^+ complex and subsequent galvanic reactions led to the growth of spiky Au shells, enabling the effective isolation and detection of the model probe CV and thiram at 10 pM and 1 nM, respectively.

The enrichment capabilities of MP nanocomposites are integral to their separation applications. Using porous and high–surface–area sieving materials enhances the amount of analyte 'captured' by the nanocomposites, as opposed to non–functionalized counterparts. This facilitates the isolation of the analyte under a magnetic field and enhances the SERS signal. MOFs are frequently used as sieving materials due to their substantial surface areas, microporous structures, and dynamic pore properties.[117] They not only capture and enrich analytes but also enable the detection and, in some cases, catalytic degradation of various toxic molecules. Ma et al. (2020) demonstrated this by fabricating Fe_3O_4@Au@MIL-100(Fe) nanocomposites for the SERS-based detection and degradation of eight different dyes.[122] The study found that the nanocomposites selectively detected cationic dyes while not interacting with anionic dyes, resulting in no SERS detection. Moreover, these materials expedited dye degradation in the presence of

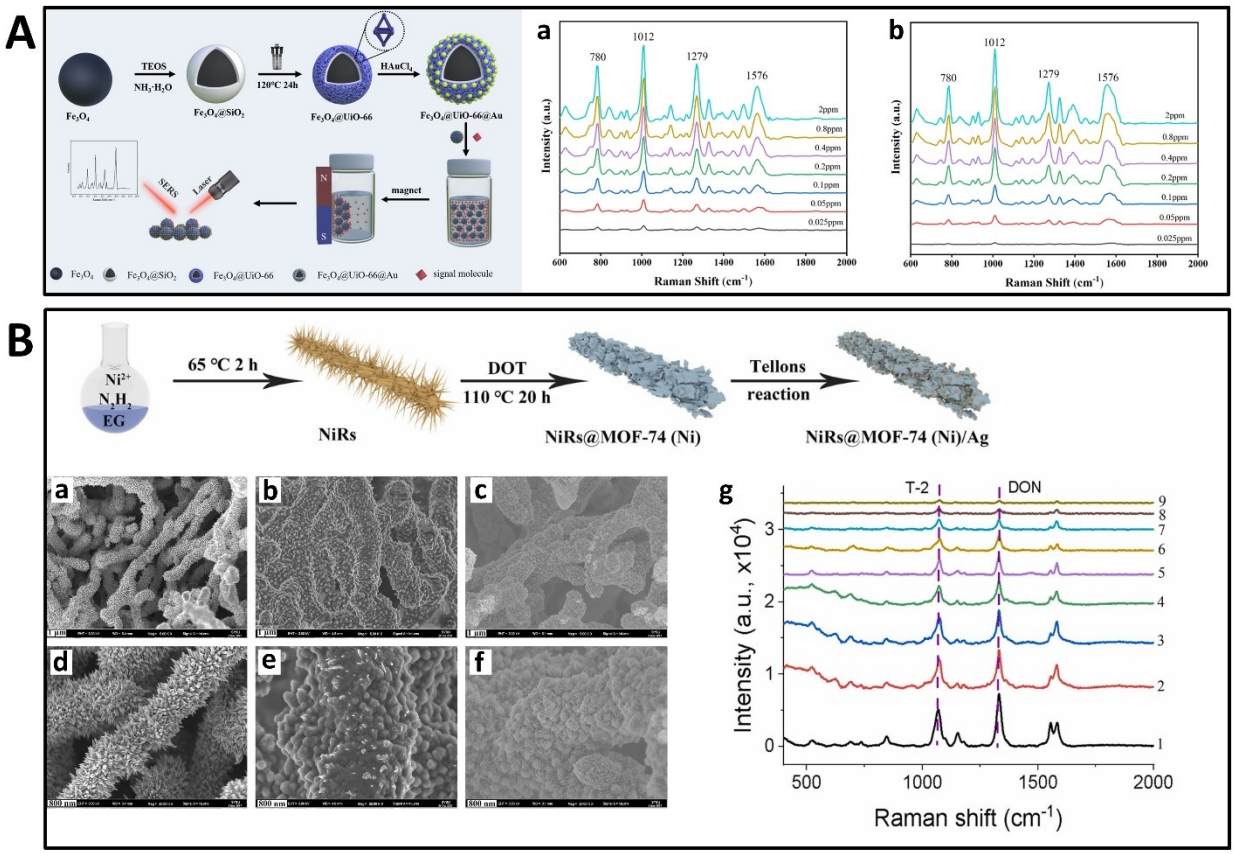

Figure 10. A) Schematic illustration of the preparation Process for Fe_3O_4@UiO-66-NH_2@Au, and SERS-based detection of TBZ: SERS spectra of TBZ in (a) apple juice and (b) grape juice. Adapted with permission from ref.[235] Copyright 2022 American Chemical Society. B) Schematic illustration of preparation of NiRs@MOF-74 (Ni)/Ag for simultaneous SERS analysis of T-2 and DON: SEM images of Ni rods (a–d), NiRs@MOF-74(Ni) (b–e), and NiRs@MOF-74(Ni)/Ag (c–f). SERS intensity (g) of T-2 and DON at different concentration. Adapted with permission from ref.[118] Copyright 2023 Elsevier.

H_2O_2, highlighting a slower degradation process in their absence.

5.2. Environmental Monitoring

MP nanocomposites are crucial in SERS-based monitoring of various environmental pollutants, including drug molecules,[9b] heavy metals,[123] pesticides,[59,124] and other toxic materials.[125] Drug molecules like antibiotics and agonists, extensively used in treating animal diseases, can accumulate in the environment and animal bodies, posing a threat to human health through the food chain.[126] MP nanocomposites offer promising solutions for concentrating, detecting, and monitoring such molecules. For instance, Tu et al. (2023) engineered core–satellite MP nanocomposites using Au@Ag nanoparticles on a Fe_3O_4 core. They employed a lateral flow immunoassay (LFA) for SERS-based detection of drugs such as kanamycin, ractopamine, clenbuterol, and chloramphenicol (Figure 11B).[127] The study achieved rapid drug detection with limits as low as pg mL^{-1} within approximately 35 minutes. In another study, Berganza et al. (2022) fabricated anisotropic magnetic nanorods, coated them with SiO_2, and functionalized them with Au nanoparticles for ciprofloxacin (CIP) detection in water.[128] The nanocomposites enabled effective concentration of CIP under a magnetic field, enhancing the SERS signal for detection limits as low as 100 nM.

Heavy metal ions, including As, Hg, Zn, and Cu, are significant environmental contaminants.[129] Particularly, Hg2+ ions are notorious for their neurotoxic effects.[130] A study involving $CoFe_2O_4$@Ag nanocomposites achieved remarkable sensitivity in Hg2+ detection down to 0.84 pM.[89] The nanocomposites, functionalized with thiol group–modified ssDNA, were combined with single–walled carbon nanotubes (SWCNTs) acting as Raman labels. In the presence of Hg^{2+}, the ssDNA captured the ions, decreasing the SWCNT signal and enabling low–concentration Hg^{2+} detection via indirect SERS. Chen et al. (2021) also focused on Hg^{2+} detection using Fe_3O4@Ag nanocomposites, functionalized with 2,5-dimercapto-1,3,4-thiadiazole (DMcT), achieving a detection limit of approximately 0.2 ppb.[131]

MP nanocomposites are effective in controlling the release of volatile molecules as well. For instance, Tian et al. (2023) coated Fe_3O_4 microparticles with Au nanorods and nanoparticles for the SERS-based detection of volatile nicotine from snus products.[132] By loading the nanocomposites into capillaries and varying storage conditions, the study found that higher temperature and humidity significantly accelerated

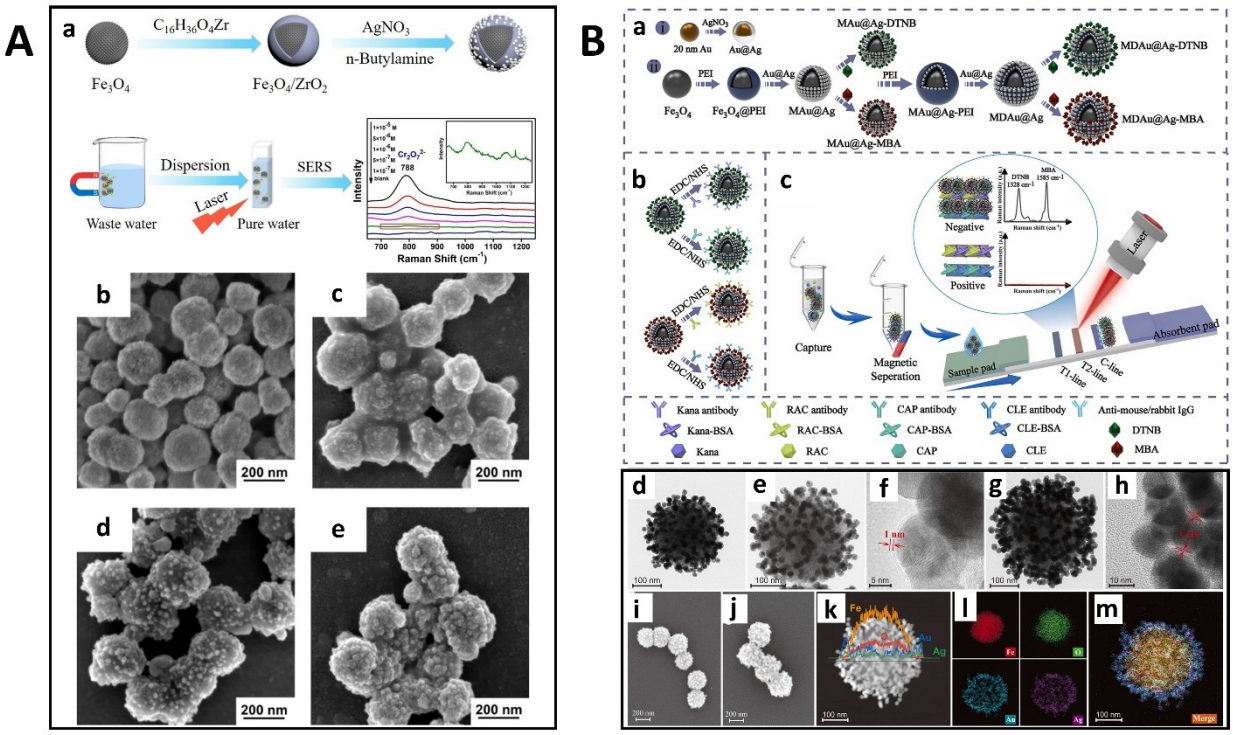

Figure 11. A) Schematic illustration (a) of the fabrication of Fe_3O_4/ZrO_2/Ag nanocomposites as effective SERS substrates for magnetic separation and Cr(VI) detection in water with low detection limits, FESEM images of the nanocomposites synthesized by increased silver precursor ($AgNO_3$) concentrations (b) 0 mM, (c) 3.92 mM, (d) 7.84 mM, (e) 11.76 mM. Adapted with permission from ref.[243] Copyright 2021 Elsevier. B) Schematic presentation of (a) synthesize of RAMAN dyes labeled magnetic–plasmonic (Fe_3O_4@Au@Ag) nanocomposites, (b) modification of their surfaces with immune SERS tags, and (c) their utilization as LFA for simultaneous detections of different types of drug residues, high–resolution TEM (HRTEM) images of (d) Fe_3O_4@Au@Ag, (e, f) Fe_3O_4@Au@Ag@PEI, (g) Fe_3O_4@Au@Ag@PEI@Au@Ag, and (h) Au@Ag particles, SEM images of (i) Fe_3O_4@Au@Ag and (j) Fe_3O_4@Au@Ag@PEI@Au@Ag, and (k–m) their EDS mapping images. Adapted with permission from ref.[127] Copyright 2023 Elsevier.

nicotine release, evidenced by an increase in the SERS signal. This showcases the versatility of MP nanocomposites in monitoring a wide range of environmental pollutants.

5.3. Biological Applications

MP nanocomposites are extensively utilized in biological applications,[133] particularly for drug delivery, photothermal applications, and SERS-based detection of sensitive biological structures like proteins and DNA. Their use in viral sensing has become increasingly popular, although it is less common compared to traditional methods like colorimetric strip tests due to the latter's rapid results. However, the advantages of SERS-based detection using MP nanocomposites, such as magnetic focusing and separation capabilities, enable the detection of viral pathogens at very low concentrations. Lee et al. (2018) demonstrated this by detecting influenza virus A with MP nanocomposites, achieving a detection limit of 7.27 fg ml^{-1}.[106c] In another study, Wang et al. (2023) functionalized magnetic beads with ssDNA and Ag nanoparticles to detect genes related to African swine fever virus down to 10 fM.[134]

MP nanocomposites are also effective in detecting infectious bacteria at low concentrations. You et al. (2020) produced Au nanoparticle–coated starch magnetic beads (AuNP@SMBs) and isolated *E. coli* O_{157}:H_7 bacteria from the environment, detecting them in the range of 100 to 10^5 CFU mL^{-1} (Figure 12A).[135] Zhao et al. (2022) utilized aptamer–conjugated MP nanocomposites for SERS-based detection and elimination of *S. aureus*, achieving a detection limit of 25 CFU mL^{-1} and utilizing photothermal principles for bacterial elimination.[109]

The dual–functionality of MP nanocomposites for both detection and therapeutic (theragnostic) applications is increasingly recognized. Kulpa–Greszta et al. (2022) investigated Fe_3O_4@APTES–Ag heterostructures for SERS-based detection and antimicrobial activity, detecting R6G dye down to 0.01 μM and demonstrating significant toxicity against *Pseudomonas aeruginosa*.[136]

For disease biomarker detection, MP nanocomposites show great promise. Alzheimer's disease (AD), characterized by the accumulation of amyloid β (Aβ) and tau proteins, is a major health concern. Demeritte et al. (2015) used core–shell MP nanocomposites functionalized on a graphene oxide layer for the detection of Aβ and tau proteins, achieving detection limits of 0.312 ng mL^{-1} for Aβ and 0.15 ng mL^{-1} for tau protein.[137] Maurer et al. (2020) functionalized Au nanoparticles with DTNB and monoclonal anti–tau antibodies, detecting tau protein at concentrations of 1 μg μL^{-1} (Figure 12B).[138] Parkinson's disease, marked by changes in dopamine levels, can also be monitored

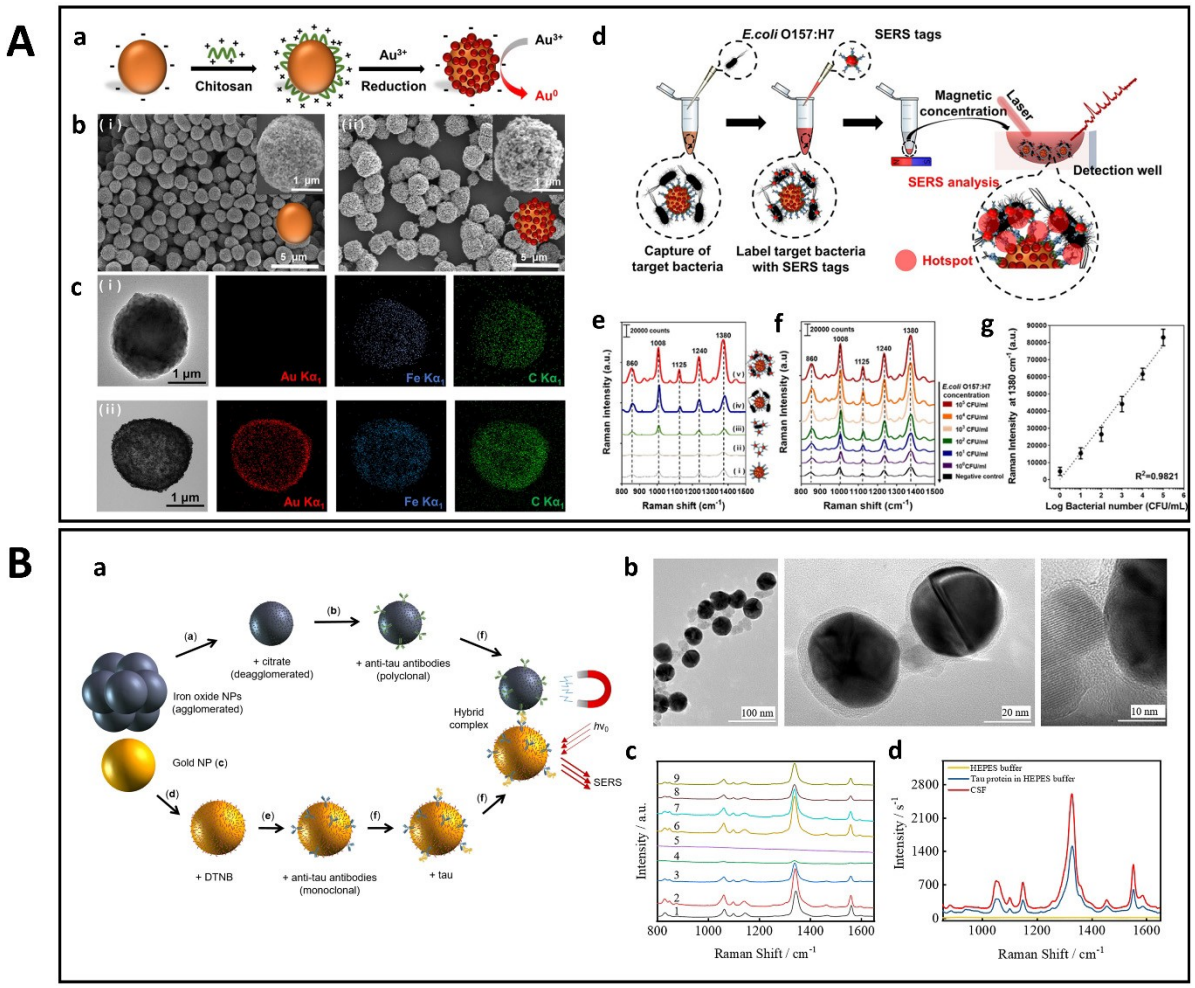

Figure 12. A) Schematic presentation (a) of the synthesis of Au NP@SMBs by electrostatic attachment of chitosan and chemical reduction of Au^{3+}, (b) SEM images of SMBs and Au NPs coated SBMs particles, (c) TEM images and elemental mapping of SMBs and AuNP@SMBs, (d) schematic depiction of the application of immuno–AuNP@SMBs for the detection of captured bacteria strain, (e) SERS spectra of nanocomposites and SERS tags in the absence (i, ii) and presence (iii–v) of E. coli O157:H7, (f) SERS spectra of nanocomposites with E.coli at different concentrations, (g) the intensity of SERS peak at 1380 cm^{-1} versus bacterial concentrations. Adapted with permission from ref.[135] Copyright 2020 American Chemical Society. B) Schematic illustration (a) of the magnetic–plasmonic hybrid complex for the SERS-based detection of tau proteins, (b) TEM images of the hybrid structures, (c) SERS signals of DTNB on Au NPs during the different synthesize/modification stages, (d) SERS spectra of structures in the absence and presence of tau protein. Adapted with permission from ref.[138] Copyright 2020 John Wiley and Sons.

using MP nanocomposites. Michałowska et al. (2022) detected dopamine with $(Fe_3O_4@Au)@SiO_2$ nanocomposites down to a concentration of 2.3×10^{-10} M.[139]

6. Summary and Outlook

This review highlights the exceptional potential of magneto–plasmonic nanocomposites in SERS applications. These nanocomposites, which integrate magnetic and plasmonic properties, provide a dynamic and versatile platform that greatly enhances the sensitivity, selectivity, and versatility of SERS-based detection and analysis. The synergy between the magnetic and plasmonic components of these materials offers numerous advantages, from precise analyte manipulation to amplified electromagnetic field effects, thus making them highly promising for future applications.

The future of MP nanocomposites in SERS applications is bright, with ongoing advancements in their synthesis, functionalization, and tailored design. These nanoarchitectures are poised to catalyze transformative breakthroughs across diverse fields such as ultra–sensitive disease diagnosis, environmental monitoring, and materials science innovation. MP nanocomposites are at the forefront of groundbreaking research and offer limitless possibilities for SERS-based technologies, potentially paving the way for a new era in advanced analytics.

The journey of integrating MP nanocomposites into practical SERS applications is not without its challenges. One of the primary hurdles is the synthesis and functionalization of these nanocomposites, which requires precise control over their size, shape, and surface properties for optimal performance. Additionally, ensuring the stability and reproducibility of SERS signals from these nanocomposites is crucial, as variations in synthesis can lead to inconsistent results, a critical issue for

practical and reliable applications. In biological applications, particularly, the biocompatibility and potential toxicity of MP nanocomposites pose significant concerns. There is a pressing need to develop safer and more biocompatible materials for medical diagnostics and therapeutics. Moreover, the integration of these nanocomposites with existing detection technologies and platforms is another critical area that needs innovative solutions. Efficient and user–friendly analytical devices that can incorporate these nanocomposites are essential for their widespread adoption.

Furthermore, the cost of production and scalability of MP nanocomposites are significant challenges for their broader application. Developing cost–effective and scalable synthesis methods will be key to their expanded use across various domains.

Looking ahead, MP nanocomposites have the potential to revolutionize various fields. In disease diagnostics, they could enable ultra–sensitive detection methods, crucial for early and accurate diagnosis. In environmental monitoring, their application could lead to more effective and precise detection of pollutants and hazardous substances, significantly contributing to environmental conservation and safety. The field of materials science also stands to benefit from the advancements in MP nanocomposites, potentially leading to the development of new materials with unique properties and wide–ranging applications. Additionally, interdisciplinary research involving MP nanocomposites is likely to increase, merging concepts from nanotechnology, chemistry, biology, and environmental science. This collaborative approach could yield innovative solutions to complex challenges, further expanding the scope and impact of MP nanocomposites in SERS-based technologies.

In conclusion, while there are challenges to overcome, the potential of MP nanocomposites in SERS and beyond is immense. With continued research and development, these obstacles can be addressed, opening the door to groundbreaking advancements and a new era in analytical technology.

Acknowledgements

This research was supported by the projects PID2020-120306RB-I00 and PID2020-113704RB-I00 (funded by MCIN/AEI/10.13039/501100011033), PDC2021-121787-I00 (funded by MCIN/AEI/10.13039/501100011033 and European Union Next Generation EU/PRTR), 2020SGR00166 (funded by Generalitat de Cataluña) and 2021PFR-URV-B2-02 (funded by Universitat Rovira I Virgili).

Conflict of Interests

The authors declare no conflict of interest.

Data Availability Statement

Data sharing is not applicable to this article as no new data were created or analyzed in this study.

Keywords: Magnetic materials · Magneto–plasmonic nanocomposites · Plasmonic materials · SERS

[1] a) S. Schlücker, *Angew. Chem. Int. Ed.* **2014**, *53*, 4756–4795; b) J. Langer, D. Jimenez de Aberasturi, J. Aizpurua, R. A. Alvarez-Puebla, B. Auguié, J. J. Baumberg, G. C. Bazan, S. E. J. Bell, A. Boisen, A. G. Brolo, J. Choo, D. Cialla-May, V. Deckert, L. Fabris, K. Faulds, F. J. García de Abajo, R. Goodacre, D. Graham, A. J. Haes, C. L. Haynes, C. Huck, T. Itoh, M. Käll, J. Kneipp, N. A. Kotov, H. Kuang, E. C. Le Ru, H. K. Lee, J.-F. Li, X. Y. Ling, S. A. Maier, T. Mayerhöfer, M. Moskovits, K. Murakoshi, J.-M. Nam, S. Nie, Y. Ozaki, I. Pastoriza-Santos, J. Perez-Juste, J. Popp, A. Pucci, S. Reich, B. Ren, G. C. Schatz, T. Shegai, S. Schlücker, L.-L. Tay, K. G. Thomas, Z.-Q. Tian, R. P. Van Duyne, T. Vo-Dinh, Y. Wang, K. A. Willets, C. Xu, H. Xu, Y. Xu, Y. S. Yamamoto, B. Zhao, L. M. Liz-Marzán, *ACS Nano* **2020**, *14*, 28–117.

[2] R. A. Álvarez-Puebla, *J. Phys. Chem. Lett.* **2012**, *3*, 857–866.

[3] a) T. Zorlu, M. A. Correa-Duarte, R. A. Alvarez-Puebla, *J. Chem. Phys.* **2023**, *158*; b) I. B. Becerril-Castro, V. Salgueiriño, M. A. Correa-Duarte, R. A. Alvarez-Puebla, *Adv. Funct. Mater.* **2023**.

[4] a) M. Blanco-Formoso, M. Turino, B. Rivas-Murias, L. Guerrini, A. Shavel, R. De La Rica, M. Correa-Duarte, V. Salgueiriño, N. Pazos-Perez, R. A. Alvarez-Puebla, *J. Phys. Chem. C* **2020**, *124*, 3270–3276; b) R. A. Alvarez-Puebla, D. J. Ross, G. A. Nazri, R. F. Aroca, *Langmuir* **2005**, *21*, 10504–10508.

[5] a) B. H. Jun, M. S. Noh, J. Kim, G. Kim, H. Kang, M. S. Kim, Y. T. Seo, J. Baek, J. H. Kim, J. Park, *Small* **2010**, *6*, 119–125; b) F. Liu, Y. Li, Y. Huang, A. Tsyrenova, K. Miller, L. Zhou, H. Qin, S. Jiang, *Nano Lett.* **2020**, *20*, 8773–8780; c) T. A. Larson, J. Bankson, J. Aaron, K. Sokolov, *Nanotechnology* **2007**, *18*, 325101; d) V. Amendola, M. Meneghetti, O. M. Bakr, P. Riello, S. Polizzi, D. H. Anjum, S. Fiameni, P. Arosio, T. Orlando, C. de Julian Fernandez, *Nanoscale* **2013**, *5*, 5611–5619.

[6] M. Ravichandran, G. Oza, S. Velumani, J. T. Ramirez, F. Garcia-Sierra, N. B. Andrade, A. Vera, L. Leija, M. A. Garza-Navarro, *Sci. Rep.* **2016**, *6*, 34874.

[7] P. Wu, X. Sun, N. Hao, L. Wang, J. Huang, J. Tang, *Spectrochim. Acta Part A* **2023**, *302*, 123101.

[8] a) S. L. Kitaw, Y. S. Birhan, H.-C. Tsai, *Environ. Res.* **2023**, 115247; b) R. Contreras-Cáceres, S. Abalde-Cela, P. Guardia-Girós, A. Fernández-Barbero, J. Pérez-Juste, R. A. Alvarez-Puebla, L. M. Liz-Marzán, *Langmuir* **2011**, *27*, 4520–4525.

[9] a) M. S. Kim, B. C. Park, Y. J. Kim, J. H. Lee, T. M. Koo, M. J. Ko, Y. K. Kim, *Small* **2020**, *16*, 2001103; b) K.-H. Huynh, E. Hahm, M. S. Noh, J.-H. Lee, X.-H. Pham, S. H. Lee, J. Kim, W.-Y. Rho, H. Chang, D. M. Kim, *Nanomaterials* **2021**, *11*, 1215.

[10] a) F. Zhang, Y. Wang, B. Yang, J. Liu, Y. Yuan, S. Bi, *Spectrochim. Acta Part A* **2023**, 123375; b) N. Sunil, R. Unnathpadi, B. Pullithadathil, *ACS Applied Nano Materials* **2023**, *6*, 11334–11350; c) B. Bhadrapriya, A. Akshaya, M. Rahul, A. Saha, S. Thomas, N. Kalarikkal, *J. Nanopart. Res.* **2023**, *25*, 47.

[11] a) H. Xu, N. Tong, L. Cui, Y. Lu, H. Gu, *J. Magn. Magn. Mater.* **2007**, *311*, 125–130; b) I. Tanabe, T. Tatsuma, *Nano Lett.* **2012**, *12*, 5418–5421.

[12] a) F. Wetz, K. Soulantica, M. Respaud, A. Falqui, B. Chaudret, *Mater. Sci. Eng. C* **2007**, *27*, 1162–1166; b) A. V. Kabashin, P. Evans, S. Pastkovsky, W. Hendren, G. A. Wurtz, R. Atkinson, R. Pollard, V. A. Podolskiy, A. V. Zayats, *Nat. Mater.* **2009**, *8*, 867–871.

[13] a) J. Dorfmuller, R. Vogelgesang, W. Khunsin, C. Rockstuhl, C. Etrich, K. Kern, *Nano Lett.* **2010**, *10*, 3596–3603; b) L. Piraux, *Applied Sciences* **2020**, *10*, 1832.

[14] a) Y. Nakatani, M. Hayashi, S. Kanai, S. Fukami, H. Ohno, *Appl. Phys. Lett.* **2016**, *108*; b) F. Mazzotta, T. W. Johnson, A. B. Dahlin, J. Shaver, S.-H. Oh, F. Hook, *ACS Photonics* **2015**, *2*, 256–262.

[15] a) Z. Hassannejad, M. E. Khosroshahi, *Opt. Mater.* **2013**, *35*, 644–651; b) M. Eid, S. El-Hallouty, M. El-Manawaty, F. Abdelzaher, M. Al-Hada, A. Ismail, *Nano-Structures&Nano-Objects* **2018**, *16*, 215–223.

[16] J. Huang, H. Wang, Z. Qi, P. Lu, D. Zhang, B. Zhang, Z. He, H. Wang, *Nano Lett.* **2021**, *21*, 1032–1039.

[17] E. A. Kwizera, E. Chaffin, Y. Wang, X. Huang, *RSC Adv.* **2017**, *7*, 17137–17153.
[18] E. S. Abu Serea, I. a Orue, J. Á. García, S. Lanceros-Méndez, J. Reguera, *ACS Applied Nano Materials* **2023**.
[19] M. S. Darwish, H. Kim, H. Lee, C. Ryu, J. Y. Lee, J. Yoon, *Nanomaterials* **2019**, *9*, 1176.
[20] A. A. Demessie, Y. Park, P. Singh, A. S. Moses, T. Korzun, F. Y. Sabei, H. A. Albarqi, L. Campos, C. R. Wyatt, K. Farsad, *Small Methods* **2022**, *6*, 2200916.
[21] J. Araújo, S. Araujo-Barbosa, A. Souza, C. Iglesias, J. Xavier, P. Souza, C. P. Cid, S. Azevedo, R. da Silva, M. Correa, *J. Phys. Chem. Solids* **2021**, *154*, 110051.
[22] a) P. Kumar, H. Khanduri, S. Pathak, A. Singh, G. Basheed, R. Pant, *Dalton Trans.* **2020**, *49*, 8672–8683; b) H. Gavilán, G. M. Rizzo, N. Silvestri, B. T. Mai, T. Pellegrino, *Nature Protocols* **2023**, *18*, 783–809.
[23] a) S. Wu, A. Sun, F. Zhai, J. Wang, W. Xu, Q. Zhang, A. A. Volinsky, *Mater. Lett.* **2011**, *65*, 1882–1884; b) D. Stanicki, L. Vander Elst, R. N. Muller, S. Laurent, *Curr. Opin. Chem. Eng.* **2015**, *8*, 7–14.
[24] a) Y. Liu, S. Jia, Q. Wu, J. Ran, W. Zhang, S. Wu, *Catal. Commun.* **2011**, *12*, 717–720; b) J. Amighian, E. Karimzadeh, M. Mozaffari, *J. Magn. Magn. Mater.* **2013**, *332*, 157–162; c) M. Farahmandjou, F. Soflaee, *Physical Chemistry Research* **2015**, *3*, 191–196.
[25] S. Hasany, I. Ahmed, J. Rajan, A. Rehman, *Nanosci. Nanotechnol* **2012**, *2*, 148–158.
[26] Z. E. Gahrouei, M. Imani, M. Soltani, A. Shafyei, *Adv. Nat. Sci. Nanosci. Nanotechnol.* **2020**, *11*, 025001.
[27] A. Díez, M. Rincón-Iglesias, S. Lanceros-Méndez, J. Reguera, E. Lizundia, *Materials Today Chemistry* **2022**, *26*, 101220.
[28] K. Sartori, F. Choueikani, A. Gloter, S. Begin-Colin, D. Taverna, B. P. Pichon, *J. Am. Chem. Soc.* **2019**, *141*, 9783–9787.
[29] D. Bokov, A. Turki Jalil, S. Chupradit, W. Suksatan, M. Javed Ansari, I. H. Shewael, G. H. Valiev, E. Kianfar, *Advances in Materials Science and Engineering* **2021**, *2021*, 1–21.
[30] a) A. Ghasemi, S. Ekhlasi, M. Mousavinia, *J. Magn. Magn. Mater.* **2014**, *354*, 136–145; b) L. Avazpour, H. Shokrollahi, M. Toroghinejad, M. Z. Khajeh, *J. Alloys Compd.* **2016**, *662*, 441–447.
[31] M. Amir, H. Gungunes, A. Baykal, M. A. Almessiere, H. Sözeri, I. Ercan, M. Sertkol, S. Asiri, A. Manikandan, *J. Supercond. Novel Magn.* **2018**, *31*, 3347–3356.
[32] L. Kaykan, J. Mazurenko, N. Ostapovych, A. Sijo, N. Y. Ivanichok, **2020**.
[33] a) P. K. Deheri, V. Swaminathan, S. D. Bhame, Z. Liu, R. V. Ramanujan, *Chem. Mater.* **2010**, *22*, 6509–6517; b) J. Sánchez, D. Cortés-Hernández, J. Escobedo-Bocardo, R. Jasso-Terán, A. Zugasti-Cruz, *J. Mater. Sci. Mater. Med.* **2014**, *25*, 2237–2242; c) D. T. T. Nguyet, N. P. Duong, T. Satoh, L. N. Anh, T. D. Hien, *J. Alloys Compd.* **2012**, *541*, 18–22.
[34] H. Rahimi, A. Ghasemi, R. Mozaffarinia, M. Tavoosi, *J. Magn. Magn. Mater.* **2017**, *444*, 111–118.
[35] X.-Y. Zhou, J. Wang, L.-L. Zhou, *J. Mater. Sci. Mater. Electron.* **2022**, *33*, 25041–25052.
[36] a) A. Jesus, J. d Jesus, R. Lima, K. Moura, J. Almeida, J. Duque, C. Meneses, *Ceram. Int.* **2020**, *46*, 11149–11153; b) S. Fayazzadeh, M. Khodaei, M. Arani, S. Mahdavi, T. Nizamov, A. Majouga, *J. Supercond. Novel Magn.* **2020**, *33*, 2227–2233; c) M. Tadic, D. Trpkov, L. Kopanja, S. Vojnovic, M. Panjan, *J. Alloys Compd.* **2019**, *792*, 599–609; d) U. Naresh, R. J. Kumar, K. C. B. Naidu, *Mater. Chem. Phys.* **2019**, *236*, 121807.
[37] M. Testa-Anta, E. Tiryaki, L. Bocher, V. Salgueiriño, *Chem. Mater.* **2022**, *34*, 11026–11038.
[38] N. Torres-Gómez, O. Nava, L. Argueta-Figueroa, R. García-Contreras, A. Baeza-Barrera, A. R. Vilchis-Nestor, *J. Nanomater.* **2019**, *2019*.
[39] a) L. M. Cursaru, R. M. Piticescu, D. V. Dragut, I. A. Tudor, V. Kuncser, N. Iacob, F. Stoiciu, *Nanomaterials* **2020**, *10*, 85; b) H. Khurshid, W. Li, S. Chandra, M.-H. Phan, G. C. Hadjipanayis, P. Mukherjee, H. Srikanth, *Nanoscale* **2013**, *5*, 7942–7952; c) Z. Nemati, J. Alonso, H. Khurshid, M. Phan, H. Srikanth, *RSC Adv.* **2016**, *6*, 38697–38702.
[40] X. Ni, J. Zhang, L. Zhao, F. Wang, H. He, P. Dramou, *J. Phys. Chem. Solids* **2022**, *169*, 110855.
[41] a) T. Amrillah, *Cryst. Growth Des.* **2022**, *22*, 4640–4660; b) A. Rana, S. Pathak, D.-K. Lim, S.-K. Kim, R. Srivastava, S. N. Sharma, R. Verma, *ACS Applied Nano Materials* **2023**, *6*, 8106–8134.
[42] a) A. Loiseau, V. Asila, G. Boitel-Aullen, M. Lam, M. Salmain, S. Boujday, *Biosensors* **2019**, *9*, 78; b) X. Lu, M. Rycenga, S. E. Skrabalak, B. Wiley, Y. Xia, *Annu. Rev. Phys. Chem.* **2009**, *60*, 167–192; c) H. Wang, X. Qiao, J. Chen, S. Ding, *Colloids Surf. A* **2005**, *256*, 111–115; d) T. M. D. Dang, T. T. T. Le, E. Fribourg-Blanc, M. C. Dang, *Adv. Nat. Sci. Nanosci. Nanotechnol.* **2011**, *2*, 015009.
[43] J. Turkevich, P. C. Stevenson, J. Hillier, *Discuss. Faraday Soc.* **1951**, *11*, 55–75.
[44] a) P. Dobrowolska, A. Krajewska, M. Gajda-Rączka, B. Bartosewicz, P. Nyga, B. J. Jankiewicz, *Materials* **2015**, *8*, 2849–2862; b) Z. Babaei Afrapoli, R. Faridi Majidi, B. Negahdari, G. Tavoosidana, *Nanomedicine Research Journal* **2018**, *3*, 190–196.
[45] N. Pazos-Perez, J. M. Fitzgerald, V. Giannini, L. Guerrini, R. A. Alvarez-Puebla, *Nanoscale Advances* **2019**, *1*, 122–131.
[46] a) X. Sun, J. Yang, L. Sun, G. Yang, C. Liu, Y. Tao, Q. Cheng, C. Wang, H. Xu, Q. Zhang, *ACS Nano* **2022**, *16*, 19174–19186; b) M. Q. He, Y. Ai, W. Hu, L. Guan, M. Ding, Q. Liang, *Adv. Mater.* **2023**, 2211915.
[47] a) J. Singh, R. Soni, D. D. Nguyen, V. K. Gupta, P. Nguyen-Tri, *Chemosphere* **2023**, *339*, 139735; b) L. Marinescu, D. Ficai, A. Ficai, O. Oprea, A. I. Nicoara, B. S. Vasile, L. Boanta, A. Marin, E. Andronescu, A.-M. Holban, *Int. J. Mol. Sci.* **2022**, *23*, 5982.
[48] J. Hao, M. He, B. Liu, J. Yang, *Chemosensors* **2022**, *10*, 373.
[49] a) Hemlata, P. R. Meena, A. P. Singh, K. K. Tejavath, *ACS Omega* **2020**, *5*, 5520–5528; b) J. S. Boruah, C. Devi, U. Hazarika, P. V. B. Reddy, D. Chowdhury, M. Barthakur, P. Kalita, *RSC Adv.* **2021**, *11*, 28029–28041; c) A. Roy, C. Pandit, A. Gacem, M. S. Alqahtani, M. Bilal, S. Islam, M. J. Hossain, M. Jameel, *Bioinorg. Chem. Appl.* **2022**, *2022*; d) R. R. Patel, S. K. Singh, M. Singh, *Materials Advances* **2023**, *4*, 1831–1849; e) D. Hebbalalu, J. Lalley, M. N. Nadagouda, R. S. Varma, *ACS Sustainable Chem. Eng.* **2013**, *1*, 703–712; f) R. Baigorri, J. M. García-Mina, R. F. Aroca, R. A. Alvarez-Puebla, *Chem. Mater.* **2008**, *20*, 1516–1521; g) J. D. S. dos Santos, R. A. Alvarez-Puebla, J. O. N. Oliveira, R. F. Aroca, *J. Mater. Chem.* **2005**, *15*, 3045–3049.
[50] a) T. Kathiraven, A. Sundaramanickam, N. Shanmugam, T. Balasubramanian, *Applied Nanoscience* **2015**, *5*, 499–504; b) A. Arya, V. Mishra, T. S. Chundawat, *Chemical Data Collections* **2019**, *20*, 100190; c) K. Araya-Castro, T.-C. Chao, B. Durán-Vinet, C. Cisternas, G. Ciudad, O. Rubilar, *Processes* **2020**, *9*, 78; d) A. B. Hashkavayi, S. Hashemnia, S. Osfouri, S. Zarei, *J. Electrochem. Soc.* **2019**, *166*, B969; e) P. B. Santhosh, J. Genova, H. Chamati, *Chemistry* **2022**, *4*, 345–369; f) M. Bayat, M. Zargar, E. Chudinova, T. Astarkhanova, E. Pakina, *Molecules* **2021**, *26*, 5402; g) G. Debnath, P. Das, A. K. Saha, *Bionanoscience* **2019**, *9*, 611–619.
[51] a) S. Batool, Z. Hussain, M. B. K. Niazi, U. Liaqat, M. Afzal, *J. Drug Delivery Sci. Technol.* **2019**, *52*, 403–414; b) G. Asnag, A. Oraby, A. Abdelghany, *Composites Part B* **2019**, *172*, 436–446.
[52] T. T. Nguyen, F. Mammeri, S. Ammar, *in Nanomaterials, Vol. 8*, **2018**.
[53] C. Fan, S. Zhu, H. Xin, Y. Tian, E. Liang, *J. Opt.* **2017**, *19*, 015401.
[54] P. Guardia, S. Nitti, M. E. Materia, G. Pugliese, N. Yaacoub, J. M. Greneche, C. Lefevre, L. Manna, T. Pellegrino, *J. Mater. Chem. B* **2017**, *5*, 4587–4594.
[55] H.-Q. Nguyen, D. Hwang, S. Park, M.-C. T. Nguyen, S. S. Kang, V. T. Tran, J. Lee, *ACS Nano* **2022**, *16*, 5795–5806.
[56] a) R. Ghorbani-Vaghei, H. Veisi, M. H. Aliani, P. Mohammadi, B. Karmakar, *J. Mol. Liq.* **2021**, *327*, 114868; b) W. Yang, L. Wei, T. Yan, M. Cai, *Catalysis Science, Technology* **2017**, *7*, 1744–1755.
[57] a) F. Li, Z. Yu, L. Zhao, T. Xue, *RSC Adv.* **2016**, *6*, 10352–10357; b) E. R. Riva, I. Pastoriza-Santos, A. Lak, T. Pellegrino, J. Pérez-Juste, V. Mattoli, *J. Colloid Interface Sci.* **2017**, *502*, 201–209; c) M. Spuch-Calvar, L. Rodríguez-Lorenzo, M. P. Morales, R. A. Álvarez-Puebla, L. M. Liz-Marzán, *J. Phys. Chem. C* **2009**, *113*, 3373–3377.
[58] D. Caruntu, B. L. Cushing, G. Caruntu, C. J. O'Connor, *Chem. Mater.* **2005**, *17*, 3398–3402.
[59] M. Blanco-Formoso, M. Turino, B. Rivas-Murias, L. Guerrini, A. Shavel, R. de la Rica, M. Correa-Duarte, V. Salgueiriño, N. Pazos-Perez, R. A. Alvarez-Puebla, *J. Phys. Chem. C* **2020**, *124*, 3270–3276.
[60] a) J. Lin, W. Zhou, A. Kumbhar, J. Wiemann, J. Fang, E. Carpenter, C. O'connor, *J. Solid State Chem.* **2001**, *159*, 26–31; b) S. Majetich, T. Wen, R. Booth, *ACS Nano* **2011**, *5*, 6081–6084; c) J. Tian, F. Zheng, H. Zhao, *J. Phys. Chem. C* **2011**, *115*, 3304–3312.
[61] P. Wang, J. H. Huh, J. Lee, K. Kim, K. J. Park, S. Lee, Y. Ke, *Adv. Mater.* **2019**, *31*, 1901364.
[62] a) S. M. Silva, R. Tavallaie, L. Sandiford, R. D. Tilley, J. J. Gooding, *Chem. Commun.* **2016**, *52*, 7528–7540; b) N. Eyvazzadeh, A. Shakeri-Zadeh, R. Fekrazad, E. Amini, H. Ghaznavi, S. Kamran Kamrava, *Lasers in medical science* **2017**, *32*, 1469–1477.
[63] a) P. Quaresma, I. Osório, G. Dória, P. A. Carvalho, A. Pereira, J. Langer, J. P. Araújo, I. Pastoriza-Santos, L. M. Liz-Marzán, R. Franco, *RSC Adv.* **2014**, *4*, 3659–3667; b) Q. Wei, H.-M. Song, A. P. Leonov, J. A. Hale, D. Oh, Q. K. Ong, K. Ritchie, A. Wei, *J. Am. Chem. Soc.* **2009**, *131*, 9728–9734.

[64] D. T. L. Alexander, D. Forrer, E. Rossi, E. Lidorikis, S. Agnoli, G. D. Bernasconi, J. Butet, O. J. F. Martin, V. Amendola, *Nano Lett.* **2019**, *19*, 5754–5761.

[65] V. Amendola, S. Scaramuzza, S. Agnoli, S. Polizzi, M. Meneghetti, *Nanoscale* **2014**, *6*, 1423–1433.

[66] P. Mohan, M. Takahashi, K. Higashimine, D. Mott, S. Maenosono, *Langmuir* **2017**, *33*, 1687–1694.

[67] a) L. Wang, Z. Wang, L. Li, J. Zhang, J. Liu, J. Hu, X. Wu, Z. Weng, X. Chu, J. Li, *RSC Adv.* **2020**, *10*, 2661–2669; b) N. T. Trang, T. T. Thuy, K. Higashimine, D. M. Mott, S. Maenosono, *Plasmonics* **2013**, *8*, 1177–1184; c) V.-T. Hoang, L. T. Tufa, J. Lee, M. Q. Doan, N. H. Anh, A.-T. Le, *J. Alloys Compd.* **2023**, *933*, 167649; d) Z. Fan, D. Senapati, S. A. Khan, A. K. Singh, A. Hamme, B. Yust, D. Sardar, P. C. Ray, *Chemistry–A European Journal* **2013**, *19*, 2839–2847.

[68] a) A. Shumskaya, I. Korolkov, A. Rogachev, Z. Ignatovich, A. Kozlovskiy, M. Zdorovets, M. Anisovich, M. Bashouti, A. Shalabny, R. Busool, *Colloids Surf. A* **2021**, *626*, 127077; b) M.-C. Yang, A. Hardiansyah, Y.-W. Cheng, H.-L. Liao, K.-S. Wang, A. Randy, C. Harito, J.-S. Chen, R.-J. Jeng, T.-Y. Liu, *Spectrochim. Acta Part A* **2022**, *281*, 121578.

[69] a) E. A. Kwizera, E. Chaffin, X. Shen, J. Chen, Q. Zou, Z. Wu, Z. Gai, S. Bhana, R. O'Connor, L. Wang, *J. Phys. Chem. C* **2016**, *120*, 10530–10546; b) A. Billen, A. de Cattelle, J. K. Jochum, M. J. Van Bael, J. Billen, J. W. Seo, W. Brullot, G. Koeckelberghs, T. Verbiest, *Physica B: Condensed Matter* **2019**, *560*, 85–90.

[70] Y. Yang, X. Jiang, J. Chao, C. Song, B. Liu, D. Zhu, Y. Sun, B. Yang, Q. Zhang, Y. Chen, *Sci. China Mater.* **2017**, *60*, 1129–1144.

[71] E. E. Bedford, C. Méthivier, C.-M. Pradier, F. Gu, S. Boujday, *Nanomaterials* **2020**, *10*, 2136.

[72] C. S. Levin, C. Hofmann, T. A. Ali, A. T. Kelly, E. Morosan, P. Nordlander, K. H. Whitmire, N. J. Halas, *ACS Nano* **2009**, *3*, 1379–1388.

[73] P. Gould, *Mater. Today* **2004**, *7*, 36–43.

[74] a) L. Li, A. Zhao, D. Wang, H. Guo, H. Sun, Q. He, *J. Nanopart. Res.* **2016**, *18*, 1–10; b) M. Sun, A. Zhao, D. Wang, J. Wang, P. Chen, H. Sun, *Nanotechnology* **2018**, *29*, 165302.

[75] a) S. Pal, J. Sharma, H. Yan, Y. Liu, *Chem. Commun.* **2009**, 6059–6061; b) I. Choi, H. D. Song, S. Lee, Y. I. Yang, T. Kang, J. Yi, *J. Am. Chem. Soc.* **2012**, *134*, 12083–12090.

[76] X. Luo, X. Zhao, G. Q. Wallace, M.-H. Brunet, K. J. Wilkinson, P. Wu, C. Cai, C. G. Bazuin, J.-F. Masson, *ACS Appl. Mater. Interfaces* **2021**, *13*, 6545–6556.

[77] H. Chen, H. Hu, C. Tao, R. M. Clauson, I. Moncion, X. Luan, S. Hwang, A. Sough, K. Sansanaphongpricha, J. Liao, H. J. Paholak, N. O. Stevers, G. Wang, B. Liu, D. Sun, *ACS Appl. Mater. Interfaces* **2019**, *11*, 23858–23869.

[78] Y. Wang, Y. Liu, Y. Li, D. Xu, X. Pan, Y. Chen, D. Zhou, B. Wang, H. Feng, X. Ma, *Research, 2020*.

[79] P. Benzo, S. Combettes, B. Pecassou, N. Combe, M. Benoit, M. Respaud, M. J. Casanove, *Physical Review Materials* **2019**, *3*, 096001.

[80] U. Tamer, İ. H. Boyacı, E. Temur, A. Zengin, İ. Dincer, Y. Elerman, *J. Nanopart. Res.* **2011**, *13*, 3167–3176.

[81] J. Li, Y. Hu, J. Yang, P. Wei, W. Sun, M. Shen, G. Zhang, X. Shi, *Biomaterials* **2015**, *38*, 10–21.

[82] A. Tomitaka, H. Arami, A. Ahmadivand, N. Pala, A. J. McGoron, Y. Takemura, M. Febo, M. Nair, *Sci. Rep.* **2020**, *10*, 10115.

[83] B. Muzzi, M. Albino, A. Gabbani, A. Omelyanchik, E. Kozenkova, M. Petrecca, C. Innocenti, E. Balica, A. Lavacchi, F. Scavone, C. Anceschi, G. Petrucci, A. Ibarra, A. Laurenzana, F. Pineider, V. Rodionova, C. Sangregorio, *ACS Appl. Mater. Interfaces* **2022**, *14*, 29087–29098.

[84] E. Fantechi, A. G. Roca, B. Sepúlveda, P. Torruella, S. Estradé, F. Peiró, E. Coy, S. Jurga, N. G. Bastús, J. Nogués, V. Puntes, *Chem. Mater.* **2017**, *29*, 4022–4035.

[85] Q. Sun, Z. Wang, B. Liu, F. He, S. Gai, P. Yang, D. Yang, C. Li, J. Lin, *Coord. Chem. Rev.* **2022**, *451*, 214267.

[86] H. Su, C. A. Hurd Price, L. Jing, Q. Tian, J. Liu, K. Qian, *Materials Today Bio* **2019**, *4*, 100033.

[87] J. Yan, K. Chaudhary, S. Chul Bae, J. A. Lewis, S. Granick, *Nat. Commun.* **2013**, *4*, 1516.

[88] B. Bharti, O. D. Velev, *Langmuir* **2015**, *31*, 7897–7908.

[89] J. Song, B. Wu, Z. Zhou, G. Zhu, Y. Liu, Z. Yang, L. Lin, G. Yu, F. Zhang, G. Zhang, *Angew. Chem. Int. Ed.* **2017**, *56*, 8110–8114.

[90] D. Lu, S. Hou, S. Liu, Q. Xiong, Y. Chen, H. Duan, *J. Phys. Chem. C* **2022**, *126*, 14967–14975.

[91] Y. Lee, M. A. Garcia, N. A. Frey Huls, S. Sun, *Angew. Chem. Int. Ed.* **2010**, *49*, 1271–1274.

[92] J. Reguera, D. J. de Aberasturi, N. Winckelmans, J. Langer, S. Bals, L. M. Liz-Marzán, *Faraday Discuss.* **2016**, *191*, 47–59.

[93] V. Coviello, D. Forrer, V. Amendola, *ChemPhysChem* **2022**, *23*, e202200136.

[94] a) A. Guadagnini, S. Agnoli, D. Badocco, P. Pastore, R. Pilot, R. Ravelle-Chapuis, M. B. F. van Raap, V. Amendola, *ChemPhysChem* **2021**, *22*, 657–664; b) A. Guadagnini, S. Agnoli, D. Badocco, P. Pastore, D. Coral, M. B. Fernàndez van Raap, D. Forrer, V. Amendola, *J. Colloid Interface Sci.* **2021**, *585*, 267–275; c) V. Amendola, S. Scaramuzza, S. Agnoli, G. Granozzi, M. Meneghetti, G. Campo, V. Bonanni, F. Pineider, C. Sangregorio, P. Ghigna, S. Polizzi, P. Riello, S. Fiameni, L. Nodari, *Nano Res.* **2015**, *8*, 4007–4023; d) S. Scaramuzza, S. Polizzi, V. Amendola, *Nanoscale Advances* **2019**, *1*, 2681–2689; e) V. Amendola, S. Scaramuzza, L. Litti, M. Meneghetti, G. Zuccolotto, A. Rosato, E. Nicolato, P. Marzola, G. Fracasso, C. Anselmi, M. Pinto, M. Colombatti, *Small* **2014**, *10*, 2476–2486.

[95] M. Żygieło, P. Piotrowski, M. Witkowski, G. Cichowicz, J. Szczytko, A. Królikowska, *Front. Chem.* **2021**, *9*, 697595.

[96] G. A. Sotiriou, A. M. Hirt, P.-Y. Lozach, A. Teleki, F. Krumeich, S. E. Pratsinis, *Chem. Mater.* **2011**, *23*, 1985–1992.

[97] C. Liu, H. Wang, S. Xu, H. Li, Y. Lu, C. Zhu, *Chemosensors* **2023**, *11*, 347.

[98] R. S. Alves, F. A. Sigoli, I. O. Mazali, *Nanotechnology* **2020**, *31*, 505505.

[99] I. Y. Goon, L. M. H. Lai, M. Lim, P. Munroe, J. J. Gooding, R. Amal, *Chem. Mater.* **2009**, *21*, 673–681.

[100] G. Sirgedaite, M. Talaikis, G. Niaura, L. Mikoliunaite, *New J. Chem.* **2023**, *47*, 402–411.

[101] P. C. Pinheiro, S. Fateixa, A. L. Daniel-da-Silva, T. Trindade, *Sci. Rep.* **2019**, *9*, 19647.

[102] C. de la Encarnación, E. Lenzi, M. Henriksen-Lacey, B. Molina, K. Jenkinson, A. Herrero, L. Colás, P. Ramos-Cabrer, J. Toro-Mendoza, I. Orue, J. Langer, S. Bals, D. Jimenez de Aberasturi, L. M. Liz-Marzán, *J. Phys. Chem. C* **2022**, *126*, 19519–19531.

[103] a) A. Majouga, M. Sokolsky-Papkov, A. Kuznetsov, D. Lebedev, M. Efremova, E. Beloglazkina, P. Rudakovskaya, M. Veselov, N. Zyk, Y. Golovin, *Colloids Surf. B* **2015**, *125*, 104–109; b) F. Bertorelle, M. Pinto, R. Zappon, R. Pilot, L. Litti, S. Fiameni, G. Conti, M. Gobbo, G. Toffoli, M. Colombatti, *Nanoscale* **2018**, *10*, 976–984.

[104] a) J.-J. Lai, W.-R. Lai, C.-Y. Chen, S.-W. Chen, C.-L. Chiang, *J. Magn. Magn. Mater.* **2013**, *331*, 204–207; b) M. Katagiri, J. L. Cuya Huaman, T. Matsumoto, K. Suzuki, H. Miyamura, J. Balachandran, *ACS Applied Nano Materials* **2019**, *3*, 418–427; c) E. Qiu, X. Chen, D.-P. Yang, M. D. Regulacio, R. M. C. R. Ramos, Z. Luo, Y.-L. Wu, M. Lin, Z. Li, X. J. Loh, *ACS Omega* **2022**, *7*, 2031–2040; d) J. Zeng, M. Gong, D. Wang, M. Li, W. Xu, Z. Li, S. Li, D. Zhang, Z. Yan, Y. Yin, *Nano Lett.* **2019**, *19*, 3011–3018.

[105] F. Zou, H. Zhou, T. V. Tan, J. Kim, K. Koh, J. Lee, *ACS Appl. Mater. Interfaces* **2015**, *7*, 12168–12175.

[106] a) X. Zheng, J. Ye, W. Chen, X. Wang, J. Li, F. Su, C. Ding, Y. Huang, *ACS Sens.* **2022**, *7*, 3126–3134; b) M. Soroush, W. Ait Mammar, A. Wilson, H. Ghourchian, M. Salmain, S. Boujday, *Biosensors* **2022**, *12*, 799; c) J. Lee, K. Takemura, E. Y. Park, *Sens. Actuators B* **2018**, *276*, 254–261.

[107] B. Zhao, H. Liu, H. Wang, Y. Zhang, X. Wang, N. Zhou, *Biosens. Bioelectron.* **2022**, *218*, 114789.

[108] a) A. Mariño-Lopez, A. Sousa-Castillo, M. Blanco-Formoso, L. N. Furini, L. Rodríguez-Lorenzo, N. Pazos-Perez, L. Guerrini, M. Pérez-Lorenzo, M. A. Correa-Duarte, R. A. Alvarez-Puebla, *ChemNanoMat* **2019**, *5*, 46–50; b) C. Vázquez-Vázquez, B. Vaz, V. Giannini, M. Pérez-Lorenzo, R. A. Alvarez-Puebla, M. A. Correa-Duarte, *J. Am. Chem. Soc.* **2013**, *135*, 13616–13619.

[109] C. Wang, G. Xu, W. Wang, Z. Ren, C. Zhang, Y. Gong, M. Zhao, Y. Qu, W. Li, H. Zhou, Y.-Q. Li, *Biosens. Bioelectron.* **2023**, *237*, 115497.

[110] S. Jafari, H. Derakhshankhah, L. Alaei, A. Fattahi, B. S. Varnamkhasti, A. A. Saboury, *Biomed. Pharmacother.* **2019**, *109*, 1100–1111.

[111] R. Thahir, A. W. Wahab, N. L. Nafie, I. Raya, *Open Chemistry* **2019**, *17*, 963–971.

[112] Ö. Bölükbaşi, B. Yola, C. Karaman, N. Atar, M. Yola, *Microchim. Acta* **2022**, *189*.

[113] Y. Yang, G. Li, P. Wang, L. Fan, Y. Shi, *Talanta* **2022**, *243*, 123369.

[114] D. Rodríguez-San-Miguel, C. Montoro, F. Zamora, *Chem. Soc. Rev.* **2020**, *49*, 2291–2302.

[115] X. Zhao, Y. Wang, D.-S. Li, X. Bu, P. Feng, *Adv. Mater.* **2018**, *30*, 1705189.

[116] H. Lai, W. Shang, Y. Yun, D. Chen, L. Wu, F. Xu, *Microchim. Acta* **2019**, *186*, 144.

[117] Y. Sun, X. Yu, J. Hu, X. Zhuang, J. Wang, H. Qiu, H. Ren, S. Zhang, Y. Zhang, Y. Hu, *ACS Sustainable Chem. Eng.* **2022**, *10*, 8400–8410.

[118] K. Ge, Y. Hu, G. Li, *Sens. Actuators B* **2023**, *374*, 132842.
[119] M. Zhang, J. Liao, X. Kong, Q. Yu, M. Zhang, A. X. Wang, *Biosensors* **2022**, *12*, 169.
[120] X.-Y. Wang, J. Yang, L. Zhou, G. Song, F. Lu, L.-J. You, J.-M. Li, *Colloids Surf. A* **2021**, *610*, 125414.
[121] B. Zou, Y. Wang, S. Zhou, S. Yang, Y. Wang, *J. Mater. Chem. C* **2022**, *10*, 3368–3374.
[122] X. Ma, H. Liu, S. Wen, Q. Xie, L. Li, J. Jin, X. Wang, B. Zhao, W. Song, *Nanotechnology* **2020**, *31*, 315501.
[123] M. Liu, Z. Wang, S. Zong, H. Chen, D. Zhu, L. Wu, G. Hu, Y. Cui, *ACS Appl. Mater. Interfaces* **2014**, *6*, 7371–7379.
[124] a) Q. He, A. Zhao, L. Li, H. Sun, D. Wang, H. Guo, M. Sun, P. Chen, *New J. Chem.* **2017**, *41*, 1582–1590; b) I. B. Becerril-Castro, I. Calderon, N. Pazos-Perez, L. Guerrini, F. Schulz, N. Feliu, I. Chakraborty, V. Giannini, W. J. Parak, R. A. Alvarez-Puebla, *Analysis & Sensing* **2022**, *2*, e202200005.
[125] M. Lv, D.-W. Sun, H. Pu, H. Zhu, *Microchem. J.* **2022**, *183*, 108137.
[126] R. Ding, Y. Chen, Q. Wang, Z. Wu, X. Zhang, B. Li, L. Lin, *Journal of Pharmaceutical Analysis* **2022**, *12*, 355–364.
[127] J. Tu, T. Wu, Q. Yu, J. Li, S. Zheng, K. Qi, G. Sun, R. Xiao, C. Wang, *J. Hazard. Mater.* **2023**, *448*, 130912.
[128] L. B. Berganza, L. Litti, M. Meneghetti, S. Lanceros-Méndez, J. Reguera, *ACS Omega* **2022**, *7*, 45493–45503.
[129] Z. L. He, X. E. Yang, P. J. Stoffella, *J. Trace Elem. Med. Biol.* **2005**, *19*, 125–140.
[130] K. Yoshizawa, E. B. Rimm, J. S. Morris, V. L. Spate, C.-c. Hsieh, D. Spiegelman, M. J. Stampfer, W. C. Willett, *N. Engl. J. Med.* **2002**, *347*, 1755–1760.
[131] Z.-Y. Chen, A. Gupta, S. Chattopadhyay, *Sens. Actuators B* **2021**, *337*, 129788.
[132] Y. Tian, L. Zhao, Y. Pan, Z. Li, X. Shen, X. Zhang, X. Tang, X. Feng, X. Huang, *RSC Adv.* **2023**, *13*, 23130–23137.
[133] B. Zou, S. Lou, J. Duan, S. Zhou, Y. Wang, *Nanoscale* **2023**, *15*, 8424–8431.
[134] H. Wang, A. Su, C. Bao, C. Liang, W. Xu, J. Chang, S. Xu, *Talanta* **2024**, *267*, 125225.
[135] S.-M. You, K. Luo, J.-Y. Jung, K.-B. Jeong, E.-S. Lee, M.-H. Oh, Y.-R. Kim, *ACS Appl. Mater. Interfaces* **2020**, *12*, 18292–18300.
[136] M. Kulpa-Greszta, A. Tomaszewska, A. Michalicha, D. Sikora, A. Dziedzic, R. Wojnarowska-Nowak, A. Belcarz, R. Pązik, *RSC Adv.* **2022**, *12*, 27396–27410.
[137] T. Demeritte, B. P. Viraka Nellore, R. Kanchanapally, S. S. Sinha, A. Pramanik, S. R. Chavva, P. C. Ray, *ACS Appl. Mater. Interfaces* **2015**, *7*, 13693–13700.
[138] V. Maurer, C. Frank, J. C. Porsiel, S. Zellmer, G. Garnweitner, R. Stosch, *Journal of Biophotonics* **2020**, *13*, e201960090.
[139] A. Michałowska, J. Krajczewski, A. Kudelski, *Spectrochim. Acta Part A* **2022**, *277*, 121266.
[140] M. Takahashi, K. Higashimine, P. Mohan, D. M. Mott, S. Maenosono, *CrystEngComm* **2015**, *17*, 6923–6929.
[141] A. Tymoczko, M. Kamp, C. Rehbock, L. Kienle, E. Cattaruzza, S. Barcikowski, V. Amendola, *Nanoscale Horiz.* **2019**, *4*, 1326–1332.
[142] Y. Wang, Y. Liu, Y. Li, D. Xu, X. Pan, Y. Chen, D. Zhou, B. Wang, H. Feng, X. Ma, *Research* **2020**.
[143] A. Walther, A. H. Muller, *Chem. Rev.* **2013**, *113*, 5194–5261.
[144] S. Hwang, T. D. Nguyen, S. Bhaskar, J. Yoon, M. Klaiber, K. J. Lee, S. C. Glotzer, J. Lahann, *Adv. Funct. Mater.* **2020**, *30*, 1907865.
[145] S. K. Smoukov, S. Gangwal, M. Marquez, O. D. Velev, *Soft Matter* **2009**, *5*, 1285–1292.

Manuscript received: November 29, 2023
Accepted manuscript online: January 31, 2024
Version of record online: February 19, 2024